

Morphogen-regulated contact-mediated signaling between cells can drive the transitions underlying body segmentation in vertebrates

Chandrashekar Kuyyamudi,^{1,2} Shakti N. Menon,¹ and Sitabhra Sinha^{1,2}

¹*The Institute of Mathematical Sciences, CIT Campus, Taramani, Chennai 600113, India*

²*Homi Bhabha National Institute, Anushaktinagar, Mumbai 400 094, India*

We propose a unified mechanism that reproduces the sequence of dynamical transitions observed during somitogenesis, the process of body segmentation during embryonic development, that is invariant across all vertebrate species. This is achieved by combining inter-cellular interactions mediated via receptor-ligand coupling with global spatial heterogeneity introduced through a morphogen gradient known to occur along the anteroposterior axis. Our model reproduces synchronized oscillations in the gene expression in cells at the anterior of the presomitic mesoderm (PSM) as it grows by adding new cells at its posterior, followed by traveling waves and subsequent arrest of activity, with the eventual appearance of somite-like patterns. This framework integrates a boundary-organized pattern formation mechanism, which uses positional information provided by a morphogen gradient, with the coupling-mediated self-organized emergence of collective dynamics, to explain the processes that lead to segmentation.

I. INTRODUCTION

The process of development in biological organisms crucially involves the self-organized emergence of spatial patterns [1]. One of the most ubiquitous of such patterns is manifest during somitogenesis, i.e., the formation of somites, which are the modular building blocks of all vertebrate bodies [2–4]. Somites compose bilaterally symmetric segments that are formed in the paraxial, or presomitic, mesoderm (PSM) of developing embryos as the body axis itself elongates [5]. Analogous processes have been implicated in the body segmentation of some invertebrates [6, 7]. Although there is great variability across species in terms of the number of somites, the mean size of a somite and the duration over which they are formed, nonetheless a conserved set of features characterizing somitogenesis is seen across these species [8]. A general conceptual model for explaining these core features is provided by the Clock and Wavefront (CW) framework proposed by Cooke and Zeeman in 1976 [9], that allows the translation of a temporal sequence into a spatial pattern [10]. They assumed the PSM to comprise cellular oscillators (clocks) which are each arrested at their instantaneous state of activity upon encountering a wavefront that moves from the anterior to the posterior of the PSM [11–18].

In order to construct an explicit mechanism embodying the CW framework, we need to disaggregate its components that operate at different length scales, namely, (i) the cellular scale at which oscillations occur, (ii) the inter-cellular scale at which contact-mediated signaling takes place, and (iii) the scale of the PSM across which morphogen gradients form and act as the environment that could modulate the inter-cellular interactions. This resonates with the proposal of Oates [19] to view the CW framework as a three-tier process. In the bottom tier, we observe oscillations at the level of a single cell in the PSM, arising from the periodic expression of clock genes [20–27]. The middle tier describes the mechanism

by which the cellular oscillators coordinate their activity with that of their neighbors. This occurs through juxtacrine signaling brought about by interactions between Notch receptors and Delta ligands [23, 28–39]. Indeed, several earlier models have explored the role of Notch-Delta coupling in bringing about robust synchronization between the oscillators [40–45]. Finally, processes that bring about the slowing down (and eventual termination) of the oscillations [20, 33, 46], and the subsequent differentiation of the cells into rostral and caudal halves of the somites [47], constitute the top tier.

In this paper we propose a model that integrates these different length scales by investigating genetic oscillators interacting via Notch-Delta coupling whose strength is modulated in a position-dependent manner due to a morphogen concentration gradient along the anteroposterior (AP) axis of the PSM. This provides a unified framework for explaining the dynamical transitions observed during somitogenesis. As the PSM expands along the AP axis through the addition of new cells at the tail [5], it is reasonable to restrict our attention to the process of somitogenesis taking place along a one-dimensional array of coupled cells in the PSM. From the perspective of our modeling which explicitly investigates the role of morphogen gradient in coordinating somite formation, the array of cells is considered to be aligned along the AP axis, as the various morphogens that are expressed along the PSM are known to form concentration gradients along this axis [48]. These primarily include molecules belonging to the FGF (Fibroblast Growth Factor) [49, 50], RA (Retinoic Acid) [51, 52] and Wnt (Wingless/integrated) families [53–55]. Even though the role of gradients on the overall dynamics has been explored [56–59], there is to date no consensus as to the explicit mechanism through which they contribute to somite formation. Our model demonstrates that if the morphogen gradient is considered to regulate the impact of the Notch intracellular domain (NICD) on the expression of the clock genes, it can lead to qualitatively different kinds of dynamics along

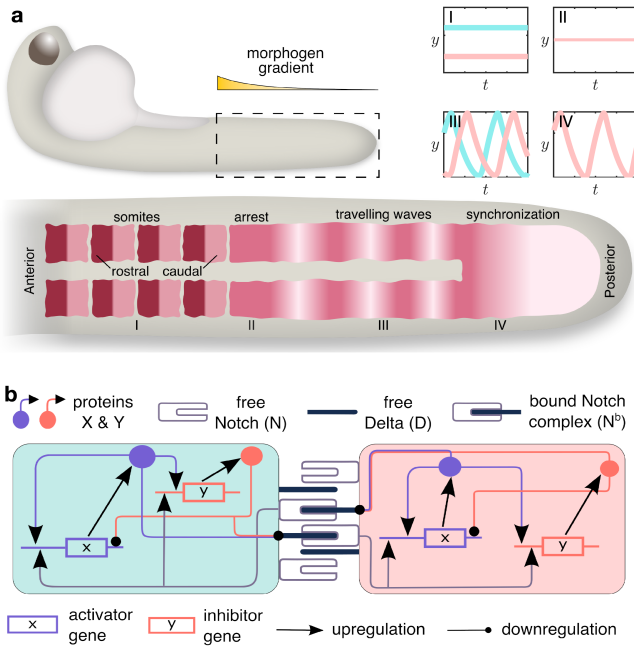


FIG. 1. The key dynamical features of somitogenesis (top) that are reproduced in our mathematical model (bottom). (a) Schematic diagram depicting the zebrafish presomitic mesoderm (PSM) and the dynamical states exhibited by the cells over the course of somitogenesis. The box outlined with broken lines represents the posterior region which exhibits a spatial gradient in morphogen concentration, represented by the exponentially varying profile shown above the box. The dynamics of the cells at the tail (region IV) are characterized by exact synchronization of the periodic variation in gene expression. As the cells move towards the anterior, they first exhibit travelling waves of gene expression (III), followed by arrest of the oscillations (II). Eventually the cells differentiate (I) into alternating bands corresponding to rostral and caudal halves of the mature somites. The figures in the insets at the right display typical time series in each of the regimes I-IV of the inhibitor gene expression for two neighboring cells coupled to each other. (b) Schematic diagram describing the interaction between two cells via Notch-Delta coupling. In general, each cell has Notch receptors, as well as, Delta ligands that bind to them. The *cis* form of the binding leads to the loss of receptors and ligands without resulting in any downstream signaling, whereas *trans* Notch-Delta binding gives rise to cleavage of the Notch Intra-Cellular Domain (NICD). The latter acts as a transcription factor (TF) for the downstream activator (x) and inhibitor (y) genes which are the essential constituents of each cellular oscillator. The proteins X and Y resulting from the expression of these genes, in turn, downregulate the production of Delta ligands (the repression being indicated by arrows with circular heads).

the PSM in a threshold-dependent manner [Fig. 1 (a)]. The dynamical evolution of our model culminates with the emergence of somites, each comprising two cells, that resemble the empirically observed segments that occur towards the tail end of the mesoderm [60, 61]. Unlike the conventional boundary-organized pattern formation

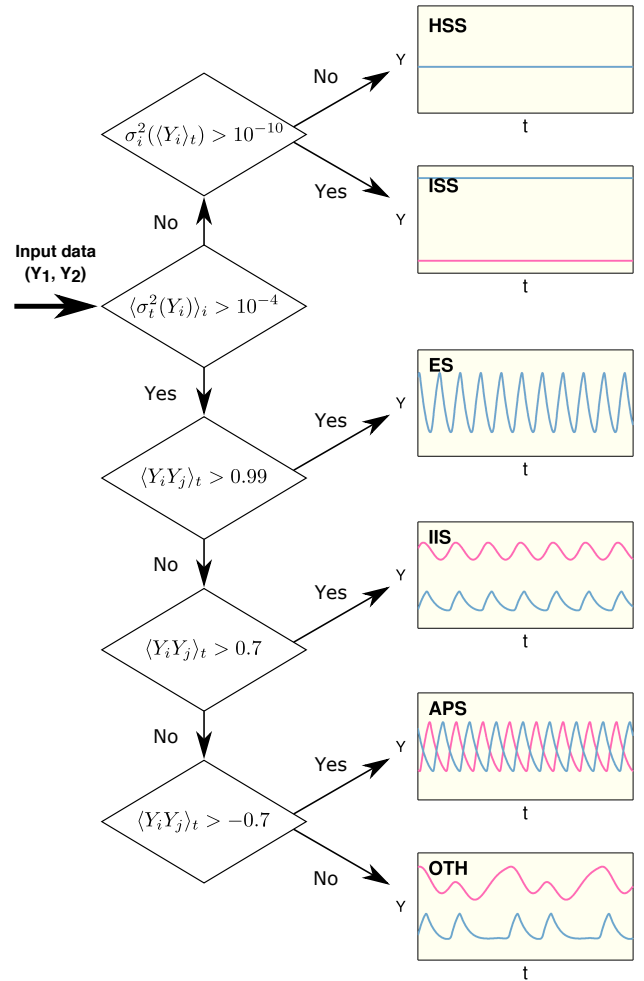


FIG. 2. Flow chart illustrating the algorithm used to classify the collective dynamical patterns obtained for a system of two coupled oscillators. To distinguish between oscillating and non-oscillating patterns, we use $\langle \sigma_t^2(Y_i) \rangle_i$ which is the mean temporal variance of the time series of Y , the concentration of the protein product of gene y , calculated over the two oscillators. To determine whether the steady states that the oscillators have reached are the same (corresponding to HSS) or different (corresponding to ISS), we compute the variance of the mean values for the two time series, $\sigma_t^2(\langle Y_i \rangle_t)$. To distinguish between the oscillating patterns, we use the equal time linear correlation between the two time series, $\langle Y_i Y_j \rangle_t$. The classification is robust with respect to small changes in the values of the thresholds, which are displayed in the figure.

paradigm [62], here the morphogen gradient does not determine the cell fate so much as affect the interaction between neighboring cells that lead to dynamical transitions similar to those observed in somitogenesis. This is in contrast to previous work where spatial heterogeneity introduced by the morphogen gradient is incorporated through variations in the autonomous oscillatory behavior of individual cells [63, 64]. Also, while it has been suggested that the mechanical deformations that the tissue

undergoes during development could play a role in somitogenesis [65, 66], our work shows that its broad features can be explained exclusively by the interactions between cells and the morphogen signal. While earlier studies have reproduced the different spatio-temporal patterns that arise over the course of somite formation [67–69], the significance of the model presented here centers around demonstrating that morphogen gradients may play a crucial role in regulating inter-cellular Notch-Delta mediated interactions, whose role in somitogenesis has been established experimentally [70, 71]. Thus, our results help address an open question as to how morphogen gradients influence the collective dynamics of the cellular oscillators by differentially modulating the inter-cellular coupling both in space and time.

II. METHODS

A. Modeling genetic oscillators interacting via Notch-Delta coupling

Several experiments have established that the cells in the presomitic mesoderm (PSM) have “clock” genes whose expression levels oscillate [20–25, 27]. In our model, we consider a generic two component genetic oscillator comprising an activator gene (x), which upregulates its own expression, as well as that of an inhibitor gene (y), which suppresses the expression of the activator gene [72]. The dynamics of this two-component oscillator can be expressed in terms of a pair of rate equations describing the change in concentrations of the protein products X and Y of genes x and y , respectively (which, in the case of zebrafish, can be identified with the *her1* and *her7* genes [19, 40]). The model parameters are chosen such that X and Y exhibit limit cycle oscillations (see Supplementary Information, Fig. S1).

As the communication between cells in the PSM is crucial in mediating their collective behavior during somitogenesis, we couple the dynamics of the clock genes of neighboring cells. Experiments have established the role of the Notch-Delta juxtacrine signaling pathway in mediating the interaction between cells that are in physical contact with each other [23, 28–37]. Such a receptor-ligand based mechanism is crucial for allowing communication between cells during processes such as somitogenesis, as gene products (proteins or mRNA) are too large to be transported across the cellular membrane, thereby preventing direct interaction between cells via diffusion [73]. In general, each cell has both Notch receptors as well as Delta ligands on their surface. A Notch receptor on cell i which is bound to a Delta ligand belonging to a neighboring cell j (i.e., *trans* binding) leads to the cleavage of NICD that will act as transcription factor for downstream genes in cell i [74, 75]. In our model, following Refs.[40, 42], NICD upregulates the expression of both the clock genes, while the gene products X, Y suppress the production of Delta ligands by the cell. We de-

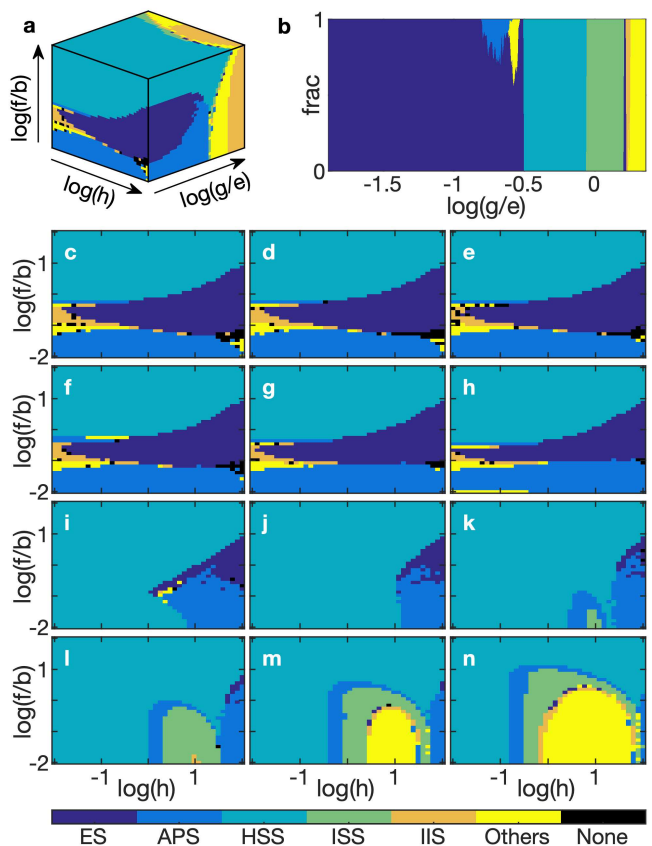


FIG. 3. Transitions between patterns representing different stages in somitogenesis seen in the collective dynamics of a pair of cells on varying the parameters governing the strength of Notch-Delta coupling in our model. (a) Schematic diagram of the three-dimensional space spanned by the coupling parameters (f, g, h), scaled by the relevant kinetic parameters of the individual oscillators. Note the logarithmic scale used for the ranges of the parameters. (b) The variation with g of the relative frequency of occurrence of patterns belonging to each of six distinct categories, viz., Exact Synchronization (ES), Anti-Phase Synchronization (APS), Homogeneous Steady States (HSS), Inhomogeneous Steady States (ISS), Inhomogeneous In-phase Synchronization (IIS) and Other dynamical patterns (Others) [“None” refers to those regions of parameter space in which no single pattern dominates]. The values of the parameters f/b and h are fixed at 0.25 and 4, respectively. (c–n) The most commonly occurring dynamical patterns (i.e., obtained for $> 50\%$ of all initial conditions used) that are seen for different values of f/b and h (varying over four orders of magnitude) for 12 equally spaced values of $\log(g/e)$ between -1.89 (panel c) and 0.36 (panel n). While HSS is the most common pattern seen over this range of parameter values, focusing on how the occurrence frequency of ES varies with f, g, h indicates where a transition from synchronization to time-invariant behavior may be achieved. In all cases, initial values of the dynamical variables for each cell are independently and identically distributed uniformly over the unit interval. Unless mentioned otherwise, the following parameter values have been used for all model simulations: $a = 16.0$, $b = 200.0$, $c = 20.0$, $e = 10.0$, $\beta^N = 5.0$, $\beta^D = 100.0$, $\gamma = 1.0$, $k^{tr} = 1.0$, $k^{cis} = 1.0$ and $\mu = 1.0$.

scribe the Notch-Delta signaling mechanism through the coupled dynamics of (i) the free (unbound) Notch receptor concentration (N), (ii) the free Delta ligand (D) and (iii) the NICD which is released as a result of *trans* binding (N^b) [see the schematic diagram shown in the Supplementary Information, Fig. S3]. Thus, the dynamics of a cell i coupled to its neighbors through Notch-Delta signaling is described by the following set of equations:

$$\frac{dX_i}{dt} = \frac{a + bX_i^2 + fN_i^b}{1 + X_i^2 + Y_i^2 + N_i^b} - cX_i, \quad (1)$$

$$\frac{dY_i}{dt} = \frac{eX_i^2 + g_i(t)N_i^b}{1 + X_i^2 + N_i^b} - Y_i, \quad (2)$$

$$\frac{dN_i}{dt} = \beta^N - \gamma N_i - k^{\text{cis}} D_i N_i - k^{\text{tr}} D^{\text{tr}} N_i, \quad (3)$$

$$\frac{dN_i^b}{dt} = k^{\text{tr}} D^{\text{tr}} N_i - \mu N_i^b, \quad (4)$$

$$\frac{dD_i}{dt} = \frac{\beta^D}{1 + h(X_i^2 + Y_i^2)} - \gamma D_i - k^{\text{cis}} D_i N_i - k^{\text{tr}} D_i N^b \quad (5)$$

Here the terms D^{tr} and N^{tr} are the mean values of D_j and N_j over all neighboring cells j to which i is coupled through *trans*-binding. The functional form chosen for the terms corresponding to binding interactions in Eqs. (1), (2), and (5) represent the fact that the transcription factors compete with each other to bind to the same site in the regulatory regions of the genes coding for X , Y and D , respectively. While the values of the model parameters can, in general, vary across cells, we restrict our attention to the spatio-temporal variation of the coupling parameter g [subscripted with the cell index in Eqn. (2)], which determines the strength of upregulation of y by the NICD (N^b). This allows us to investigate the role of spatial heterogeneity imposed by the gradient of morphogen concentration along the anteroposterior (AP) axis of the PSM. For the simulations reported here we have considered the case $k^{\text{tr}} = k^{\text{cis}} = 1$. We note that our results are qualitatively unchanged in the absence of *cis*-inhibition (see Supplementary Information, Fig. S4).

B. Morphogen gradients in the PSM

It is known that the morphogens RA, Wnt and FGF are differentially expressed along the PSM, exhibiting monotonically varying concentration gradients having peaks at the posterior (for FGF and Wnt) or anterior (for RA) ends [54, 77, 78]. Experiments on several vertebrate species have shown that high concentrations of RA initiate differentiation, while increased levels of Wnt and FGF, which are known to promote sustained oscillations in the expression of the clock genes, impede the formation of mature somites [49, 52, 79, 80]. Note that some aspects of the roles played by Wnt and FGF are already accounted for in the local dynamics of our model, where each cell is capable of autonomous robust oscillations. As our primary goal is to explicate the mechanisms

driving termination of oscillatory activity followed by cellular differentiation, we focus on the role of RA on the collective dynamics of cells in the PSM. We incorporate the effect of this morphogen in the spatial variation of the coupling parameter g which is assumed to exponentially decay from the anterior to the posterior end of the domain. Such a profile will naturally arise if the morphogen diffuses from a source located at the anterior and is degraded at a constant rate across space [81–83]. The regulation of the Notch-mediated interaction can come about by the binding of a morphogen molecule to a cell surface receptor leading to (either directly or indirectly) the expression of molecules that aid NICD or its downstream effector to bind more strongly to the promoter site of gene Y . This contrasts with earlier studies (e.g., see Ref. [84]) that have assumed the morphogen to regulate the gene expressing Notch, which would affect expression of both X and Y (instead of selectively affecting only Y as in the present model).

C. Dynamical evolution of the morphogen gradient

Our model focuses on the behavior of a contiguous segment of cells of length ℓ in the PSM with a morphogen source located at its anterior. If the strength of the source is constant in time, it would have resulted in the gradient becoming progressively less steep as the PSM expands. This dilution is countered by the net increase in the strength of the source through the secretion of morphogen by the newly matured somites (see Supplementary Information, Fig. S6). Thus, as the PSM expands due to addition of cells at the posterior tail, we can view the segment under consideration as effectively flowing up a morphogen gradient along the AP axis [19]. We choose a segment of N cells with a spatial extent ℓ that is initially located ($t = 0$) at the posterior end of the PSM, i.e., at the lower end of the gradient. Its evolution is followed for a duration T , the time required for the array of cells to move across the entire spatial extent of the morphogen gradient considered here. Thus, it determines the rate at which cells move along the gradient, which in turn is related to the rate at which the PSM expands by cell division at its posterior end. As mentioned above, the effect of the varying morphogen concentration on the dynamics of the cells is introduced via the coupling parameter g . Specifically, we assume that the value of g at each site is proportional to the corresponding morphogen concentration, yielding an exponentially varying gradient of g across the AP axis: $g_i(t) = g_{\text{min}} \exp(\lambda_g x_i(t))$. The steepness of the gradient is quantified by λ_g , which is a function of T , as well as g_{max} and g_{min} , which are the values of g at the anterior and posterior ends of the PSM, respectively, viz., $\lambda_g = \ln(g_{\text{max}}/g_{\text{min}})/T$. We assume that the effective flow of the segment of cells along the AP axis occurs at a uniform rate. This can be taken to be unity without loss of generality by appropriate choice of time unit. Thus, the instantaneous position $x_i(t)$ along

the gradient of the i th cell in the segment is given by $x_i(t) = t + (\ell/N)(i - 1)$, with the initial condition as $x_1(t = 0) = 0$.

III. RESULTS

In our simulations, we have considered the PSM to comprise cells, each of which exhibits oscillating gene expression. We assume a minimal model for the genetic oscillator consisting of two clock genes, one activatory and the other inhibitory, whose products correspond to fate determining proteins (see Methods). The oscillations of neighboring cells influence each other through Notch-Delta inter-cellular coupling [Fig. 1 (b)]. We have explicitly verified that incorporating delay in the contact mediated signaling does not alter our results qualitatively (see Supplementary Information, Fig. S5).

A. Dynamics of a pair of coupled cells

In the simplest setting, namely, a pair of adjacent cells, which allows us to investigate the effect of coupling on the collective dynamics, the system can exhibit a wide range of spatio-temporal patterns. These can be classified systematically through the use of quantitative measures (see Fig. 2). We focus on the patterns that can be immediately interpreted in the context of somitogenesis: (i) Inhomogeneous Steady States (ISS), (ii) Homogeneous Steady States (HSS), (iii) Anti-Phase Synchronization (APS) and (iv) Exact Synchronization (ES) [shown schematically as insets of Fig. 1 (a)]. The range of values of the coupling-related parameters f , g and h over which these patterns are observed in a pair of coupled cells are shown in Fig. 3. The parameters f and g govern the strength with which the Notch intra-cellular domain (N^b) regulates the activatory and inhibitory clock genes, respectively, while h is related to the intensity of repression of the Delta ligand (D) by each of the clock genes. As inter-cellular coupling is believed to be responsible for the synchronized activity of cells in the initial stage of somitogenesis [76], we note that the dynamical regime corresponding to ES occurs for low g and intermediate values of f , with the region increasing in size for larger h .

B. Morphogen gradient-induced heterogeneity in a pair of coupled cells

Spatial variation in these coupling parameters across the PSM can arise through heterogeneity in the underlying morphogen concentrations. Introducing heterogeneity through the coupling parameter g in the pair of adjacent cells considered earlier (g_1 and g_2 being their respective values), we observe that qualitatively similar spatio-temporal patterns to those observed in Fig. 3 are

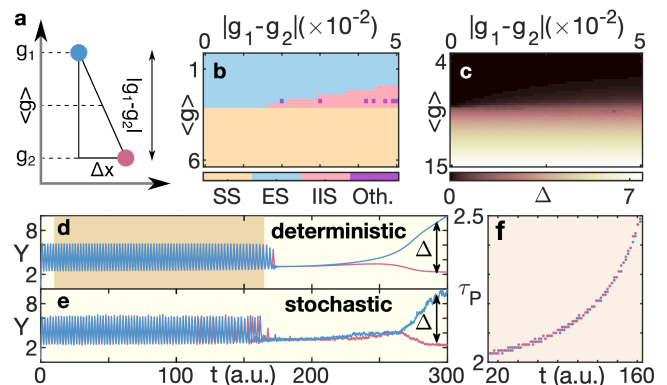


FIG. 4. Incorporating a morphogen gradient by varying the Notch-Delta coupling parameter g of adjacent oscillators reproduces the temporal sequence of patterns observed during somitogenesis. (a) Schematic representation of the spatial variation of g , resulting from the different concentrations of a morphogen sensed by neighboring cells, which are separated by a distance Δx in space. The steepness of the gradient is quantified by $|g_1 - g_2|$, the difference in the values $g_{1,2}$ for the two oscillators, while their location on the gradient is determined by the mean $\langle g \rangle$. (b) The most commonly occurring dynamical patterns (i.e., obtained for $> 50\%$ of all initial conditions used) on varying $|g_1 - g_2|$ and $\langle g \rangle$. The states of the adjacent cells, characterized by the protein concentration Y , converge to fixed points $Y_{1,2}$ in the steady state (SS) region. (c) The difference between the steady state concentrations of the adjacent cells, $\Delta = |Y_1 - Y_2|$, increases with $\langle g \rangle$ as one effectively moves up the morphogen gradient, while being relatively unaffected by the steepness $|g_1 - g_2|$. (d-f) The dynamical consequences of a morphogen gradient with an exponentially varying concentration profile. (d) As a pair of coupled cells gradually move upstream of the gradient, resulting in an increase of $g_{1,2}$ over time t , their collective behavior (represented by Y) converges from initially synchronized oscillations (ES) to an inhomogeneous steady state (ISS, characterized by finite values of Δ) at long times. These transitions are robust with respect to stochastic fluctuations (as shown in panel e). The changes occurring in the system during the transition from oscillations to steady state behavior (shaded region) can be quantitatively investigated by focusing on how the period τ_p of the oscillations changes over time. (f) As cells move upstream of the morphogen gradient (corresponding to a progression from posterior to anterior regions in the PSM), the model displays an increase in time period τ_p . This is consistent with a key experimental observation, viz., slowing of oscillations as cells approach the anterior end of the PSM, during somitogenesis. The coupling parameters are $f = 50$, $h = 4$, $g_{\max} = 15$ and $g_{\min} = 0.5$, with $\Delta x = 3$ arb. units.

obtained. On varying the mean value of the coupling $\langle g \rangle = (g_1 + g_2)/2$, which effectively represents the location of these cells on the PSM, and the steepness of the gradient $|g_1 - g_2|$ [Fig. 4 (a)], the range of $\langle g \rangle$ over which ES is seen (corresponding to the region proximal to the posterior end of the PSM) does not appear to change appreciably on increasing $|g_1 - g_2|$ [Fig. 4 (b)]. Above a critical value of $\langle g \rangle$ which is independent of the gradient,

the activities of the cells are arrested at Y_1 and Y_2 , respectively, with the gap $\Delta = |Y_1 - Y_2|$ becoming larger as we move towards the anterior end, corresponding to increasing $\langle g \rangle$ [Fig. 4 (c)].

As explained in the Methods, over the course of development, the PSM expands through new cells being added to its posterior end, such that the existing cells progressively encounter increasing values of the morphogen concentration. Modeling this time-evolution as an effective flow of the segment of adjacent cells along the gradient in g , we observe that a transient phase of ES is followed by desynchronization and subsequent attenuation of the oscillations, eventually leading to a separation of the steady states of the two cells [Fig. 4 (d); see also Supplementary Information, Fig. S7)]. The gap Δ between the steady states increases with time, giving rise to a pronounced ISS state. This duration depends sensitively on the steepness of the morphogen concentration gradient (see Supplementary Information, Fig. S8). The sequence of dynamical transitions seen in the model are robust with respect to the presence of noise as shown explicitly in Fig. 4 (e) by introducing stochastic fluctuations in the dynamical variables (see also Supplementary Information, Fig. S9). Immediately preceding the arrest of periodic activity, we observe that the period τ_P [Fig. 4 (f)] of the oscillations increases with time that is in agreement with experimental observations of somitogenesis [85, 86].

C. Dynamics of a cellular array in a growing PSM in presence of a morphogen gradient

Having seen that a pair of contiguous cells can indeed converge to markedly different steady state values of their clock gene expressions, we now investigate the generalization to a spatially extended segment of length ℓ in the growing PSM subject to a morphogen gradient [varying from g_{\min} to g_{\max} as shown schematically above Fig. 5 (a)]. As the principal variation of the morphogen concentration occurs along the AP axis of the PSM, we restrict our focus to a one-dimensional array of cells aligned along this axis. As new cells are added to the posterior of the PSM over time, the relative position of the segment of cells under consideration shifts along the morphogen gradient from the posterior to the anterior. We note that had there been a temporally invariant source of morphogen at the anterior, the expansion of the PSM would have resulted in a dilution of the gradient. However, newly matured somites at the anterior end serve as additional sources of the morphogen over time [87–89], thereby ensuring that each cell experiences an exponential increase in the morphogen concentration. This is reproduced in our model by the segment effectively flowing up the morphogen gradient (as discussed in Methods).

As shown in Fig. 5 (a), for a range of values of the parameters g_{\max} , g_{\min} and ℓ , the cells display a short-lived ES pattern, which is followed by the development of a

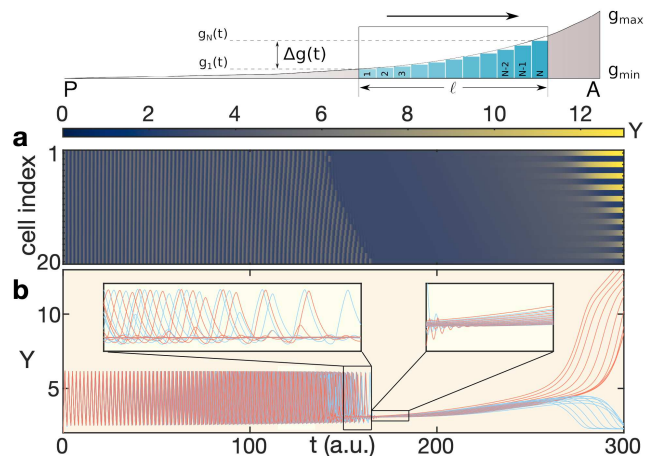


FIG. 5. Collective dynamics of a cellular array responding to an exponential gradient of morphogen concentration reproduces the spatio-temporal evolution of PSM activity seen during somitogenesis. The transition from progenitor cells in the posterior (P) to maturity at the anterior (A) of a segment of length ℓ comprising N cells in the PSM viewed as a flow upstream (moving window in the schematic on top) over a period of time T along the exponential profile of the parameter g , decaying from g_{\max} to g_{\min} , reflecting the morphogen gradient. Different cells in the window sense different morphogen concentrations, whose values change over time. This is incorporated in terms of the time-dependent gradient $\Delta g(t)$, with $g_1(t)$ and $g_N(t)$ being the values of the coupling parameter g at the anterior and posterior ends of the window at time t , respectively. The resulting change in the activity of a segment comprising $N = 20$ coupled cells, as it moves from P to A, is shown in (a). The system initially exhibits synchronized oscillations across the segment but, as a consequence of the gradient, a phase lag develops between adjacent cells (as seen in the time series in panel b, where odd and even numbered cells are represented using red and blue curves, respectively). This results in a wave-like propagation of the peak expression from the anterior to the posterior end of the segment in each cycle. Subsequently, the oscillations reduce in intensity leading to arrest of the oscillations, a magnified view of the transition being shown in the left inset of panel (b). This is followed by a divergence of the dynamical trajectories followed by the different cells, as shown in the right inset of (b). This gives way to an inhomogeneous steady state (ISS) with adjacent cells attaining different fates characterized by alternating high and low values of the protein concentration Y [cells with odd and even indices on the segment are shown using different colors in panel (b)]. Results shown are for parameter values of $g_{\max} = 15$, $g_{\min}(= g_0) = 0.5$ and $T = 300$ a.u. In all cases, initial values of the dynamical variables for each cell are independently and identically distributed uniformly over the unit interval. We note that NICD concentration at each cell exhibits qualitatively similar dynamics (see Supplementary Information, Fig. S10).

phase lag between adjacent cells [as can be seen in the inset of Fig. 5 (b)]. This is analogous to the appearance of a small phase difference between the pair of oscillators described earlier, and manifests as a travelling wave that propagates along the PSM. We note that such a traveling wave of gene expression has indeed been experimentally observed to move through the PSM towards the anterior [19, 24, 54]. As the cells move further up the gradient, the oscillations subside, eventually giving way to a heterogeneous steady state characterized by adjacent cells having alternating high and low clock gene expressions. The gap between these high and low values increases with time to eventually produce a distinctive pattern that resemble the stripes that arise due to polarization of each somite into rostral and caudal halves [as seen for large t in both Figs. 5 (a) and (b)]. In this asymptotic steady state, the separation between the high and low values for clock gene expression is greater than the amplitude of the oscillations seen at lower values of t . Thus, we can reproduce the entire sequence of dynamical transitions observed in the PSM during somitogenesis through a model incorporating an array of oscillators that interact via Notch-Delta signaling while “moving up” a morphogen gradient. We note that, in different organisms, the size of somites vary across the mesoderm, with the ones occurring at the posterior end being smaller [90] and resembling the segments consisting of pairs of cells that arise in our model. We would like to point out that the dynamics resulting from the inter-cellular interactions can yield ISS states having larger spatial periodicities, which suggests a potential for producing larger somites (see Supplementary Information, Fig. S11). We also note that introducing additional mechanisms such as lateral induction via Jagged receptors [91] or diffusive coupling between cells via gap junctions [67, 69] may allow for variation in the wavelength of the periodic pattern.

IV. DISCUSSION

Somitogenesis is seen across all vertebrates, and recent evidence implies that mechanisms underlying it could have analogues even in segmentation of invertebrates, such as arthropods [6, 92]. It would appear that there is an invariant set of mechanisms responsible for this process, that differ only in terms of the specific identities of the contributing molecular players across species. Thus, somitogenesis would in general involve (i) a cellular “clock”, (ii) means by which neighboring clocks communicate, and (iii) a spatial gradient of signaling molecules, which introduces heterogeneity in the interactions between the clocks. We have shown here that incorporating these three elements in a model of a PSM, that grows through the addition of cells at the posterior, reproduces the sequence of invariant dynamical transitions seen in somitogenesis.

While the roles of interacting clocks and that of morphogen gradients have been investigated individually in

earlier studies, we provide here a framework to understand how these two work in tandem to give rise to the key features associated with somitogenesis. In particular, our results shed light on the significance of the steepness of the morphogen gradient. For instance, we may consider the consequences of a reduction in the steepness leading to a linear profile for the morphogen gradient which can arise, for example, when the degradation rate is negligible. On replacing the exponential morphogen gradient in our model with a linear one, we observe a very long-lived transient state before the system converges to an inhomogeneous steady state. This therefore suggests that exponential gradients allow relatively rapid switching between qualitatively distinct dynamical regimes. Hence, by varying the steepness of the RA gradient experimentally it should be possible to determine how the time required for maturation changes as a consequence. This is especially true in the case of the time interval between cessation of oscillations and the polarization of the somites. As inter-cellular coupling is also known to regulate the period of the segmentation clock [93], it is possible that introducing other morphogen gradients, that influence the strength of the coupling, can explain variations in the rate at which somites form over time. The broad features observed here can be reproduced in two-dimensional cellular arrays with anisotropic inter-cellular coupling (see Supplementary Information, Fig. S12). Furthermore, the core assumption of our model, namely that Notch-Delta coupling plays a crucial role in regulating somitogenesis in the presence of a morphogen gradient can be probed in experimental systems where Notch signaling has been arrested. Future research involving incorporation of additional details in the model presented here may provide answers to several challenges that explanations of somitogenesis based on the clock-and-wavefront mechanism have faced [94].

ACKNOWLEDGMENTS

We would like to thank Krishnan Iyer, Jose Negrete Jr, Shubha Tole and Vikas Trivedi for valuable suggestions. The authors would like to acknowledge discussions during the ICTP/ICTS Winter Schools on Quantitative Systems Biology (ICTP/smr2879, ICTS/qsb2019/12). SNM has been supported by the IMSc Complex Systems Project (12th Plan), and the Center of Excellence in Complex Systems and Data Science, both funded by the Department of Atomic Energy, Government of India. The simulations and computations required for this work were supported by High Performance Computing facility (Nandadevi and Satpura) of The Institute of Mathematical Sciences, which is partially funded by DST.

- [1] A. J. Koch and H. Meinhardt. Biological pattern formation: from basic mechanisms to complex structures. *Rev Mod Phys*, 66:1481–1507, 1994.
- [2] M.-L. Dequéant and O. Pourquié. Segmental patterning of the vertebrate embryonic axis. *Nat Rev Genet*, 9(5):370, 2008.
- [3] C. Gomez, E. M. Özbudak, J. Wunderlich, D. Baumann, J. Lewis, and O. Pourquié. Control of segment number in vertebrate embryos. *Nature*, 454(7202):335, 2008.
- [4] F. J. Vonk and M. K. Richardson. Developmental biology: Serpent clocks tick faster. *Nature*, 454(7202):282, 2008.
- [5] S. F. Gilbert. *Developmental Biology*. Sinauer, 2013.
- [6] A. Stollewerk, M. Schoppmeier, and W. G. M. Damen. Involvement of notch and delta genes in spider segmentation. *Nature*, 423(6942):863, 2003.
- [7] A. F. Sarrazin, A. D. Peel, and M. Averof. A segmentation clock with two-segment periodicity in insects. *Science*, 336:338–341, 2012.
- [8] O. Pourquié and P. P. L. Tam. A nomenclature for prospective somites and phases of cyclic gene expression in the presomitic mesoderm. *Dev Cell*, 1(5):619–620, 2001.
- [9] J. Cooke and E. C. Zeeman. A clock and wavefront model for control of the number of repeated structures during animal morphogenesis. *J Theor Biol*, 58(2):455–476, 1976.
- [10] O. Pourquié. The segmentation clock: converting embryonic time into spatial pattern. *Science*, 301(5631):328–330, 2003.
- [11] R. E. Baker, S. Schnell, and P. K. Maini. A clock and wavefront mechanism for somite formation. *Dev Biol*, 293(1):116–126, 2006.
- [12] M. Santillán and M. C. Mackey. A proposed mechanism for the interaction of the segmentation clock and the determination front in somitogenesis. *PLOS ONE*, 3(2):e1561, 2008.
- [13] H. Nagahara, Y. Ma, Y. Takenaka, R. Kageyama, and K. Yoshikawa. Spatiotemporal pattern in somitogenesis: A non-turing scenario with wave propagation. *Phys Rev E*, 80(2):021906, 2009.
- [14] S. D. Hester, J. M. Belmonte, J. S. Gens, S. G. Clendenon, and J. A. Glazier. A multi-cell, multi-scale model of vertebrate segmentation and somite formation. *PLOS Comput Biol*, 7(10):e1002155, 2011.
- [15] S. Ares, L. G. Morelli, D. J. Jörg, A. C. Oates, and F. Jülicher. Collective modes of coupled phase oscillators with delayed coupling. *Phys Rev Lett*, 108(20):204101, 2012.
- [16] P. J. Murray, P. K. Maini, and R. E. Baker. Modelling delta-notch perturbations during zebrafish somitogenesis. *Dev Biol*, 373:407–421, 2013.
- [17] D. J. Jörg, L. G. Morelli, S. Ares, and F. Jülicher. Synchronization dynamics in the presence of coupling delays and phase shifts. *Phys Rev Lett*, 112:174101, 2014.
- [18] G. Wiedermann, R. A. Bone, J. C. Silva, M. Bjorklund, P. J. Murray, and J. K. Dale. A balance of positive and negative regulators determines the pace of the segmentation clock. *eLife*, 4:e05842, 2015.
- [19] A. C. Oates, L. G. Morelli, and S. Ares. Patterning embryos with oscillations: structure, function and dynamics of the vertebrate segmentation clock. *Development*, 139(4):625–639, 2012.
- [20] I. Palmeirim, D. Henrique, D. Ish-Horowicz, and O. Pourquié. Avian hairy gene expression identifies a molecular clock linked to vertebrate segmentation and somitogenesis. *Cell*, 91(5):639–648, 1997.
- [21] K. J. Dale and O. Pourquié. A clock-work somite. *Bioessays*, 22(1):72–83, 2000.
- [22] Y. Saga and H. Takeda. The making of the somite: molecular events in vertebrate segmentation. *Nat Rev Genet*, 2(11):835, 2001.
- [23] M. Maroto, J. K. Dale, M.-L. Dequeant, A.-C. Petit, and O. Pourquié. Synchronised cycling gene oscillations in presomitic mesoderm cells require cell-cell contact. *Int J Dev Biol*, 49(2-3):309–315, 2003.
- [24] Y. Masamizu, T. Ohtsuka, Y. Takashima, H. Nagahara, Y. Takenaka, K. Yoshikawa, H. Okamura, and R. Kageyama. Real-time imaging of the somite segmentation clock: revelation of unstable oscillators in the individual presomitic mesoderm cells. *Proc Natl Acad Sci USA*, 103(5):1313–1318, 2006.
- [25] I. H. Riedel-Kruse, C. Müller, and A. C. Oates. Synchrony dynamics during initiation, failure, and rescue of the segmentation clock. *Science*, 317(5846):1911–1915, 2007.
- [26] C. Schröter, S. Ares, L. G. Morelli, A. Isakova, K. Hens, D. Soroldoni, M. Gajewski, F. Jülicher, S. J. Maerkl, B. Deplancke, and A. C. Oates. Topology and dynamics of the zebrafish segmentation clock core circuit. *PLOS Biol*, 10(7):e1001364, 2012.
- [27] A. B. Webb, I. M. Lengyel, D. J. Jörg, G. Valentin, F. Jülicher, L. G. Morelli, and A. C. Oates. Persistence, period and precision of autonomous cellular oscillators from the zebrafish segmentation clock. *eLife*, 5:e08438, 2016.
- [28] Y.-J. Jiang, L. Smithers, and J. Lewis. Vertebrate segmentation: the clock is linked to notch signalling. *Curr Biol*, 8(24):R868–R871, 1998.
- [29] Z. Ferjentsik, S. Hayashi, J. K. Dale, Y. Bessho, A. Herremans, B. De Strooper, G. del Monte, J. L. de la Pompa, and M. Maroto. Notch is a critical component of the mouse somitogenesis oscillator and is essential for the formation of the somites. *PLoS Genet*, 5(9):e1000662, 2009.
- [30] A. Hubaud and O. Pourquié. Signalling dynamics in vertebrate segmentation. *Nat Rev Mol Cell Bio*, 15:709–721, 2014.
- [31] R. A. Conlon, A. G. Reaume, and J. Rossant. Notch1 is required for the coordinate segmentation of somites. *Development*, 121(5):1533–1545, 1995.
- [32] O. Pourquié. Notch around the clock. *Curr Opin Genet Dev*, 9(5):559–565, 1999.
- [33] Y.-J. Jiang, B. L. Aerne, L. Smithers, C. Haddon, D. Ish-Horowicz, and J. Lewis. Notch signalling and the synchronization of the somite segmentation clock. *Nature*, 408(6811):475, 2000.
- [34] E. C. Lai. Notch signaling: control of cell communication and cell fate. *Development*, 131:965–973, 2004.
- [35] S. S. Huppert, M. X. G. Ilagan, B. De Strooper, and R. Kopan. Analysis of notch function in presomitic mesoderm suggests a γ -secretase-independent role for presenilins in somite differentiation. *Dev Cell*, 8(5):677–688, 2005.
- [36] A. Mara and S. A. Holley. Oscillators and the emergence of tissue organization during zebrafish somitogenesis. *Trends Cell Biol*, 17(12):593–599, 2007.
- [37] R. Kageyama, Y. Masamizu, and Y. Niwa. Oscillator

- mechanism of notch pathway in the segmentation clock. *Dev Dynam*, 236(6):1403–1409, 2007.
- [38] D. Sprinzak, A. Lakhapal, L. LeBon, L. A. Santat, M. E. Fontes, G. A. Anderson, J. Garcia-Ojalvo, and M. B. Elowitz. Cis-interactions between notch and delta generate mutually exclusive signalling states. *Nature*, 465(7294):86, 2010.
- [39] D. Sprinzak, A. Lakhapal, L. LeBon, J. Garcia-Ojalvo, and M. B. Elowitz. Mutual inactivation of notch receptors and ligands facilitates developmental patterning. *PLoS Comput Biol*, 7(6):e1002069, 2011.
- [40] J. Lewis. Autoinhibition with transcriptional delay: a simple mechanism for the zebrafish somitogenesis oscillator. *Curr Biol*, 13(16):1398–1408, 2003.
- [41] F. Giudicelli and J. Lewis. The vertebrate segmentation clock. *Curr Opin Genet Dev*, 14:0–414, 2004.
- [42] K. Horikawa, K. Ishimatsu, E. Yoshimoto, S. Kondo, and H. Takeda. Noise-resistant and synchronized oscillation of the segmentation clock. *Nature*, 441(7094):719, 2006.
- [43] F. Giudicelli, E. M. Özbudak, G. J. Wright, and J. Lewis. Setting the tempo in development: an investigation of the zebrafish somite clock mechanism. *PLoS Biol*, 5(6):e150, 2007.
- [44] H. B. Tiedemann, E. Schneltzer, S. Zeiser, B. Hoesel, J. Beckers, G. K. H. Przemek, and M. H. de Angelis. From dynamic expression patterns to boundary formation in the presomitic mesoderm. *PLoS Comput Biol*, 8(6):e1002586, 2012.
- [45] H. B. Tiedemann, E. Schneltzer, S. Zeiser, W. Wurst, J. Beckers, G. K. H. Przemek, M. H. de Angelis, and D. Thieffry. Fast synchronization of ultradian oscillators controlled by delta-notch signaling with cis-inhibition. *PLoS Comput Biol*, 10:e1003843, 2014.
- [46] M. J. McGrew and O. Pourquié. Somitogenesis: segmenting a vertebrate. *Curr Opin Genet Dev*, 8(4):487–493, 1998.
- [47] M. Oginuma, Y. Takahashi, S. Kitajima, M. Kiso, J. Kanno, A. Kimura, and Y. Saga. The oscillation of Notch activation, but not its boundary, is required for somite border formation and rostral-caudal patterning within a somite. *Development*, 137(9):1515–1522, 2010.
- [48] S. Gibb, M. Maroto, and J. K. Dale. The segmentation clock mechanism moves up a notch. *Trends Cell Biol*, 20(10):593–600, 2010.
- [49] J. Dubrulle, M. J. McGrew, and O. Pourquié. Fgf signaling controls somite boundary position and regulates segmentation clock control of spatiotemporal hox gene activation. *Cell*, 106(2):219–232, 2001.
- [50] J. Dubrulle and O. Pourquié. fgf8 mrna decay establishes a gradient that couples axial elongation to patterning in the vertebrate embryo. *Nature*, 427:419–422, 2004.
- [51] J. Dubrulle and O. Pourquié. Coupling segmentation to axis formation. *Development*, 131:5783–5793, 2004.
- [52] J. Vermot and O. Pourquié. Retinoic acid coordinates somitogenesis and left–right patterning in vertebrate embryos. *Nature*, 435(7039):215, 2005.
- [53] A. Aulehla. Segmentation in vertebrates: clock and gradient finally joined. *Gene Dev*, 18:2060–2067, 2004.
- [54] A. Aulehla, W. Wiegand, V. Baubet, M. B. Wahl, C. Deng, M. Taketo, M. Lewandoski, and O. Pourquié. A β -catenin gradient links the clock and wavefront systems in mouse embryo segmentation. *Nat Cell Biol*, 10(2):186, 2008.
- [55] L. Bajard, L. G. Morelli, S. Ares, J. Pécresseaux, F. Julicher, and A. C. Oates. Wnt-regulated dynamics of positional information in zebrafish somitogenesis. *Development*, 141:1381–1391, 2014.
- [56] A. Goldbeter, D. Gonze, and O. Pourquié. Sharp developmental thresholds defined through bistability by antagonistic gradients of retinoic acid and fgf signaling. *Dev Dynam*, 236(6):1495–1508, 2007.
- [57] A. Goldbeter and O. Pourquié. Modeling the segmentation clock as a network of coupled oscillations in the notch, wnt and fgf signaling pathways. *J Theor Biol*, 252(3):574–585, 2008.
- [58] K. I. Mazzitello, C. M. Arizmendi, and H. G. E. Hentschel. Converting genetic network oscillations into somite spatial patterns. *Phys Rev E*, 78(2):021906, 2008.
- [59] D. J. Jörg, A. C. Oates, and F. Jülicher. Sequential pattern formation governed by signaling gradients. *Phys Biol*, 13(5):05LT03, 2016.
- [60] B. W. Youn, R. E. Keller, and G. M. Malacinski. An atlas of notochord and somite morphogenesis in several anuran and urodelean amphibians. *Development*, 59(1):223–247, 1980.
- [61] S. Tlili, J. Yin, J.-F. Rupperecht, M. A. Mendieta-Serrano, G. Weissbart, N. Verma, X. Teng, Y. Toyama, J. Prost, and T. E. Saunders. Shaping the zebrafish myotome by intertissue friction and active stress. *Proc Natl Acad Sci USA*, 116(51):25430–25439, 2019.
- [62] A. D. Lander. Pattern, growth, and control. *Cell*, 144(6):955–969, 2011.
- [63] P. J. Murray, P. K. Maini, and R. E. Baker. The clock and wavefront model revisited. *J Theor Biol*, 283(1):227–238, 2011.
- [64] T. Tomka, D. Iber, and M. Boareto. Travelling waves in somitogenesis: Collective cellular properties emerge from time-delayed juxtacrine oscillation coupling. *Prog Biophys Mol Biol*, 137:76–87, 2018.
- [65] P. Adhyapak, A. M. Piatkowska M. J. Norman, S. G. Clendenon, C. D. Stern, J. A. Glazier, and J. M. Belmonte. A mechanical model of early somite segmentation. *iScience*, 24(4):102317, 2021
- [66] R. Narayanan, M. A. Mendieta-Serrano, and T. E. Saunders. The role of cellular active stresses in shaping the zebrafish body axis. *Curr Opin Cell Biol*, 73 : 69-77, 2021
- [67] H. Meinhardt. *Models of Biological Pattern Formation*. Academic Press, London, 1982.
- [68] P. François, V. Hakim, and E. D. Siggia. Deriving structure from evolution: metazoan segmentation. *Mol Syst Biol*, 3(1):154, 2007.
- [69] J. Cotterell, A. Robert-Moreno, and J. Sharpe. A local, self-organizing reaction-diffusion model can explain somite patterning in embryos. *Cell Syst*, 1:257–269, 2015.
- [70] K. Wahi, M. S. Bochter, and S. E. Cole. The many roles of notch signaling during vertebrate somitogenesis. *Semin Cell Dev Biol*, 49:68–75, 2016.
- [71] B.-K. Liao and A. C. Oates. Delta-notch signalling in segmentation. *Arthropod Struct Dev*, 46(3):429–447, 2017.
- [72] R. Guantes and J. F. Poyatos. Dynamical principles of two-component genetic oscillators. *PLoS Comput Biol*, 2:e30, 2006.
- [73] D. A. Goodenough and D. L. Paul. Gap junctions. *Cold Spring Harb Perspect Biol*, 1(1):a002576, 2009
- [74] C. Takke and J. A. Campos-Ortega. her1, a zebrafish pair-rule like gene, acts downstream of notch signalling to

- control somite development. *Development*, 126(13):3005–3014, 1999.
- [75] A. C. Oates and R. K. Ho. Hairy/e (spl)-related (her) genes are central components of the segmentation oscillator and display redundancy with the delta/notch signaling pathway in the formation of anterior segmental boundaries in the zebrafish. *Development*, 129(12):2929–2946, 2002.
- [76] M. Maroto, J. K. Dale, M.-L. Dequeant, A.-C. Petit, and O. Pourquie. Synchronised cycling gene oscillations in pre-somitic mesoderm cells require cell-cell contact. *Int J Dev Biol*, 49:309–315, 2005.
- [77] J. B. Gurdon and P.-Y. Bourillot. Morphogen gradient interpretation. *Nature*, 413(6858):797, 2001.
- [78] A. Aulehla and O. Pourquie. Signaling gradients during paraxial mesoderm development. *Cold Spring Harb Perspect Biol*, 2(2):a000869, 2010.
- [79] A. Sawada, M. Shinya, Y.-J. Jiang, A. Kawakami, A. Kuroiwa, and H. Takeda. Fgf/mapk signalling is a crucial positional cue in somite boundary formation. *Development*, 128(23):4873–4880, 2001.
- [80] T. A. Moreno and C. Kintner. Regulation of segmental patterning by retinoic acid signaling during xenopus somitogenesis. *Dev Cell*, 6(2):205–218, 2004.
- [81] A. D. Lander, Q. Nie, and F. Y. M. Wan. Do morphogen gradients arise by diffusion? *Dev Cell*, 2(6):785–796, 2002.
- [82] S. Bergmann, O. Sandler, H. Sberro, S. Shnider, E. Schejter, B.-Z. Shilo, and N. Barkai. Pre-steady-state decoding of the bicoid morphogen gradient. *PLoS Biol*, 5(2):1–11, 2007.
- [83] N. Barkai and B.-Z. Shilo. Robust generation and decoding of morphogen gradients. *Cold Spring Harb Perspect Biol*, 1(5), 2009.
- [84] A. Hubaud, I. Regev, L. Mahadevan, and O. Pourquie. Excitable dynamics and Yap-dependent mechanical cues drive the segmentation clock. *Cell*, 171(3):668–682, 2017.
- [85] E. A. Delaune, P. François, N. P. Shih, and S. L. Amacher. Single-cell-resolution imaging of the impact of Notch signaling and mitosis on segmentation clock dynamics. *Dev Cell*, 23(5):995–1005, 2012.
- [86] N. P. Shih, P. François, E. A. Delaune, and S. L. Amacher. Dynamics of the slowing segmentation clock reveal alternating two-segment periodicity. *Development*, 142(10):1785–1793, 2015.
- [87] R. D. del Corral, I. Olivera-Martinez, A. Goriely, E. Gale, M. Maden, and K. Storey. Opposing fgf and retinoid pathways control ventral neural pattern, neuronal differentiation, and segmentation during body axis extension. *Neuron*, 40(1):65–79, 2003.
- [88] R. D. del Corral and K. G. Storey. Opposing fgf and retinoid pathways: a signalling switch that controls differentiation and patterning onset in the extending vertebrate body axis. *Bioessays*, 26(8):857–869, 2004.
- [89] M. Rhinn and P. Dollé. Retinoic acid signalling during development. *Development*, 139(5):843–858, 2012.
- [90] C. Schröter, L. Herrgen, A. Cardona, G. J. Brouhard, B. Feldman, and A. C. Oates. Dynamics of zebrafish somitogenesis. *Dev Dynam*, 237(3):545–553, 2008.
- [91] Z. Hadjivasiliou, G. L. Hunter, and B. Baum. A new mechanism for spatial pattern formation via lateral and protrusion-mediated lateral signalling. *J Roy Soc Interface*, 13(124):20160484, 2016.
- [92] E. Clark, A. D. Peel, and M. Akam. Arthropod segmentation. *Development*, 146(18):dev170480, 2019.
- [93] L. Herrgen, S. Ares, L. G. Morelli, C. Schröter, F. Jülicher, and A. C. Oates. Intercellular coupling regulates the period of the segmentation clock. *Curr Biol*, 20(14):1244–1253, 2010.
- [94] C. D. Stern and A. M. Piatkowska. Multiple roles of timing in somite formation. *Semin Cell Dev Biol*, 42:134–139, 2015.

SUPPLEMENTARY INFORMATION FOR

Morphogen-regulated contact-mediated signaling between cells can drive the transitions underlying body segmentation in vertebrates

LIST OF SUPPLEMENTARY FIGURES

1. Fig S1: Schematic diagram of the genetic oscillator model and phase portrait of its dynamics.
2. Fig S2: Representative patterns of collective dynamics for a pair of coupled oscillators subject to a morphogen gradient.
3. Fig S3: Schematic diagram illustrating the canonical Notch signaling pathway that allows contact-mediated interaction between cells.
4. Fig S4: Relative importance of *trans* and *cis* forms of Notch-Delta binding for reproducing the observed sequence of transitions during somitogenesis.
5. Fig S5: Effect of delay in Notch-Delta mediated interaction on the collective dynamics of a pair of coupled oscillators responding to an exponential gradient of morphogen concentration cell signaling.
6. Fig S6: Temporal evolution of the concentration of a morphogen along the gradient as sensed by a particular cell in the growing PSM.
7. Fig S7: Temporal evolution of the dynamical variables in a pair of coupled oscillators responding to an exponential gradient of morphogen concentration.
8. Fig S8: The collective dynamics of a pair of coupled oscillators separated by a distance Δx responding to an exponential gradient of morphogen concentration having steepness λ_g .
9. Fig S9: Effect of noise on the collective dynamics of a pair of oscillators interacting via Notch-Delta coupling modulated by an exponential gradient of morphogen concentration.
10. Fig S10: Collective dynamics of a cellular array represented in terms of the bound Notch concentration (N^b).
11. Fig S11: The model dynamics can generate temporally invariant spatial patterns with different periodicities.
12. Fig S12: A two-dimensional cellular array can exhibit a linear sequence of alternating peaks and troughs of the protein concentration Y .

MODELING THE DYNAMICS OF CLOCK GENE EXPRESSION IN CELLS COUPLED VIA NOTCH-DELTA SIGNALING

In the model presented in the main text, we consider a two-component genetic oscillator [?], comprising an activator gene x and an inhibitor gene y . The parameter values of the model (see the next section) have been chosen such that it exhibits autonomous oscillatory activity. The interactions between these two genes are schematically shown in Fig. S1 (left). Each uncoupled oscillator consists of two variables X and Y that represent the concentrations of the products expressed by genes x and y , respectively. The trajectory of an uncoupled oscillator in the X - Y phase plane is shown in Fig. S1 (right), along with the nullclines $\dot{X} = 0$ and $\dot{Y} = 0$. Fig. S1 (left) also displays the nature of the interactions between genes x and y , where the variables N^b , N and D describe the Notch-Delta coupling between cells [2].

In a system of coupled oscillators, we observe a variety of synchronization behavior (examples of which are shown in Fig. S2). These can be categorized into 6 principal collective dynamical patterns, namely Inhomogeneous Steady State (ISS), Exact Synchronization (ES), Homogeneous Steady State (HSS), Inhomogeneous In-phase Synchronization (IIS), Anti-Phase Synchronization (APS) and Other synchronization patterns (OTH).

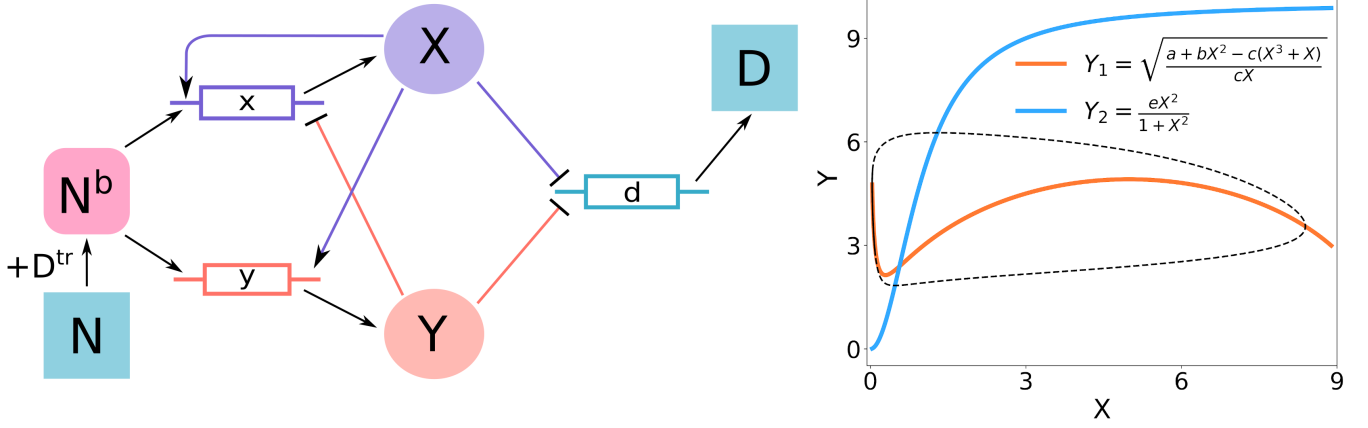


FIG. S1. **Schematic diagram of the genetic oscillator model and phase portrait of its dynamics.** [left] Schematic diagram of the interactions resulting in gene expression oscillations in the model used in the main text. The system comprises an activator gene x and an inhibitor gene y that yield the gene products X and Y , respectively. These in turn inhibit the expression of Delta gene d , resulting in suppression of the production of Delta ligands D . Each cell contains Notch receptors N that, when bound with Delta ligands from another cell, causes the Notch Intracellular Domain (NICD, represented through the proxy variable N^b) to cleave off and act as transcriptional factors that upregulate the expression of the downstream genes x and y . [right] The dynamics of expression levels X and Y for the activator and inhibitor genes, respectively, in a single uncoupled oscillator, shown in terms of the trajectory of the limit cycle (broken curve) and the nullclines (red: $\dot{X} = 0$, blue: $\dot{Y} = 0$) obtained from Eqs. (1)-(2) in the main text.

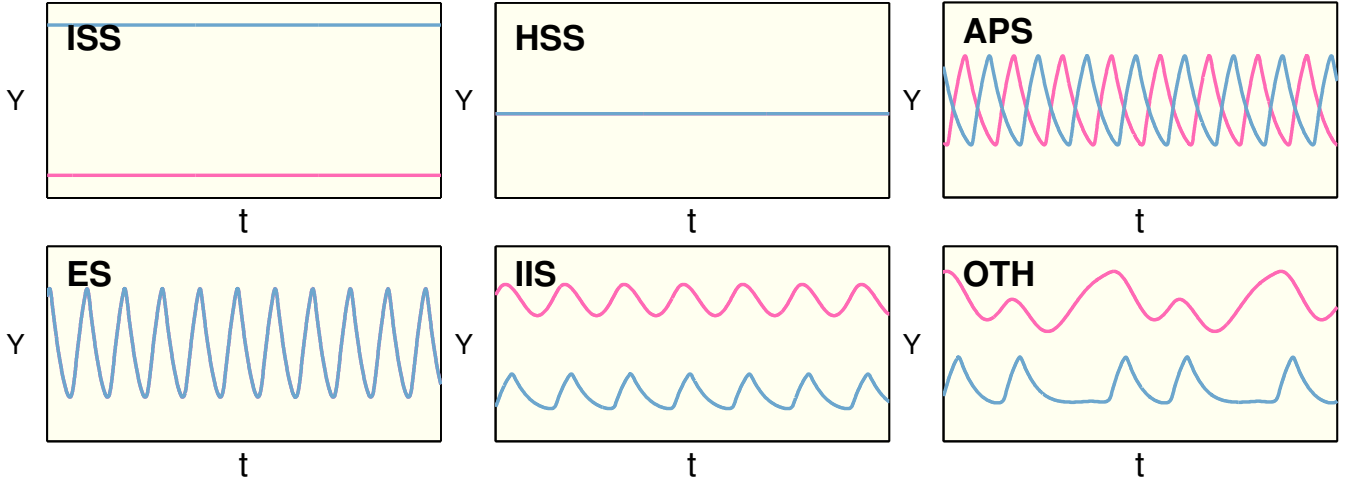


FIG. S2. **Representative patterns of collective dynamics for a pair of coupled oscillators subject to a morphogen gradient.** Typical time series of the inhibitor gene expression Y for a pair of cells coupled to each other (each exhibiting oscillations in isolation, as shown in Fig. S1). Different dynamical regimes obtained by varying the coupling parameters f , g and h that are shown here correspond to (top row, left) Inhomogeneous Steady State (ISS), (bottom row, left) Exact Synchronization (ES), (top row, center) Homogeneous Steady State (HSS), (bottom row, center) Inhomogeneous In-phase Synchronization (IIS), (top row, right) Anti-Phase Synchronization (APS) and (bottom row, right) Other synchronization patterns (OTH). The activity of the two cells are represented using two different colors in each panel. Note that the two curves overlap in the ES and HSS regimes.

MODEL PARAMETERS

As described in the main text, the time-evolution of each cell i (coupled to its neighbors via Notch-Delta coupling) is described by the following set of coupled differential equations:

$$\begin{aligned}
 \frac{dX_i}{dt} &= \frac{a + bX_i^2 + fN_i^b}{1 + X_i^2 + Y_i^2 + N_i^b} - cX_i & \frac{dY_i}{dt} &= \frac{eX_i^2 + g_i(t)N_i^b}{1 + X_i^2 + N_i^b} - Y_i \\
 \frac{dN_i}{dt} &= \beta^N - \gamma N_i - k^{\text{cis}}D_iN_i - k^{\text{tr}}D^{\text{tr}}N_i & \frac{dN_i^b}{dt} &= k^{\text{tr}}D^{\text{tr}}N_i - \mu N_i^b \\
 \frac{dD_i}{dt} &= \frac{\beta^D}{1 + h(X_i^2 + Y_i^2)} - \gamma D_i - k^{\text{cis}}D_iN_i - k^{\text{tr}}D_iN^{\text{tr}}
 \end{aligned}$$

$a = 16$ $b = 200$ $f = 50$ $c = 20$ $e = 10$
 $\beta^N = 5$ $\mu = 1$
 $h = 4$ $\beta^D = 100$ $\gamma = 1$ $k^{\text{cis}} = 1$ $k^{\text{tr}} = 1$

The model parameters, described in the table below, can be broadly classified into those that specify the properties of (i) the cellular oscillator comprising the clock genes, (ii) Notch signaling between neighboring cells that couples their respective activities, and (iii) the morphogen gradient that modulates the strength of the Notch-mediated coupling. The values chosen for each of these parameters (indicated above the corresponding equations in which they appear) are selected to ensure that the gene circuit in each cell exhibits oscillations in the absence of any coupling to neighboring cells and that the time-scale of Notch signaling dynamics is approximately the same as that of the cellular oscillator. The spatial gradient of morphogen concentration has been kept temporally invariant. Note that the parameter $g_i(t)$ which represents the strength with which Notch promotes the expression of one of the clock genes (Y) varies in space (as a result of the morphogen gradient), as well as, in time (due to the effective movement of a cell along the morphogen gradient towards the anterior because of the expansion of the PSM via the addition of new cells at its posterior end).

Parameter	Interpretation
a	Base transcription rate of gene X
b	Transcription rate of gene X on self-activation (i.e., dimer of protein expressed by X binds to promoter of gene X)
c	Degradation rate of the product of gene X
e	Transcription rate of gene Y when the dimer of protein expressed by X is bound to the promoter of gene Y
f	Transcription rate of gene X when N^b is bound to the promoter of gene X
g	Transcription rate of gene Y when N^b is bound to the promoter of gene Y
β^N	Maximal production rate of the free Notch receptors
β^D	Maximal production rate of the Delta ligands
k^{cis}	Forward rate constant for complex formation involving Notch receptor and Delta ligand of the same cell
k^{tr}	Forward rate constant for complex formation between Notch receptor of a cell and Delta ligand of its neighbor
γ	Degradation rate of the Notch receptor
μ	Degradation rate of the Notch Intracellular Domain, NICD (N^b)
h	Affinity of Delta repressing dimers of proteins expressed by X and Y for the promoter of gene coding Delta ligand

NUMERICAL SOLUTION OF THE MODEL

As the dynamics of each cell is described by a system of five coupled ordinary differential equations (ODEs), to describe the behavior of a 1D array of N cells, we solve $5N$ coupled ODEs using an adaptive numerical integrator (such as, `odeint` from the Python `scipy` module). The initial values of the dynamical variables are chosen from a uniform distribution over the unit interval $[0, 1]$.

RELATIVE CONTRIBUTIONS OF *TRANS* AND *CIS* BINDING TO THE COLLECTIVE DYNAMICS

The Notch-Delta signaling pathway (Fig. S3) provides neighboring cells in the presomitic mesoderm (PSM) a mechanism for communicating with each other. Binding of the Notch receptor of a cell to a Delta ligand belonging to a neighboring cell leads to the cleavage of the Notch intra-cellular domain (NICD) which serves as a transcription factor for downstream genes either directly or indirectly. This process is referred to as *trans*-activation of Notch to distinguish it from *cis*-inhibition in which Delta and Notch of the same cell forms a complex resulting in the ligand and the receptor no longer being available for inter-cellular communication.

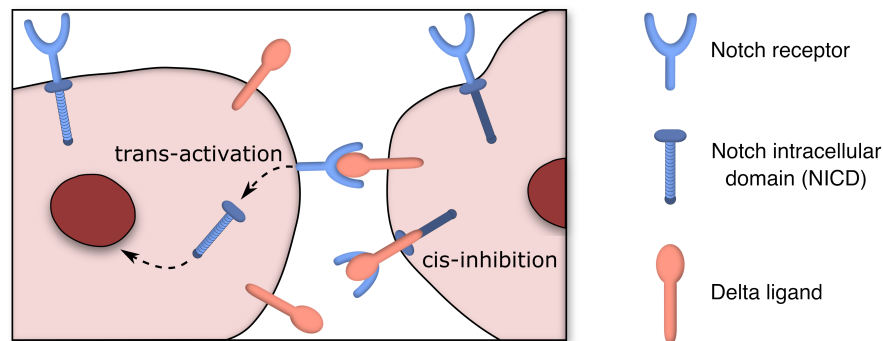


FIG. S3. Schematic diagram illustrating the canonical Notch signaling pathway that allows contact-mediated interaction between cells.

Fig. S4 demonstrates the relative importance of *trans* and *cis* forms of Notch-Delta binding in generating the sequence of dynamical transitions observed during somitogenesis. Absence of *cis*-inhibition leads to only minor, quantitative changes in the cell activity from that observed when *cis*- and *trans*-bindings both have the same propensity. However, in the absence of *trans*-activation the cells are no longer able to communicate with each other, preventing the system from exhibiting any of the transitions associated with somitogenesis.

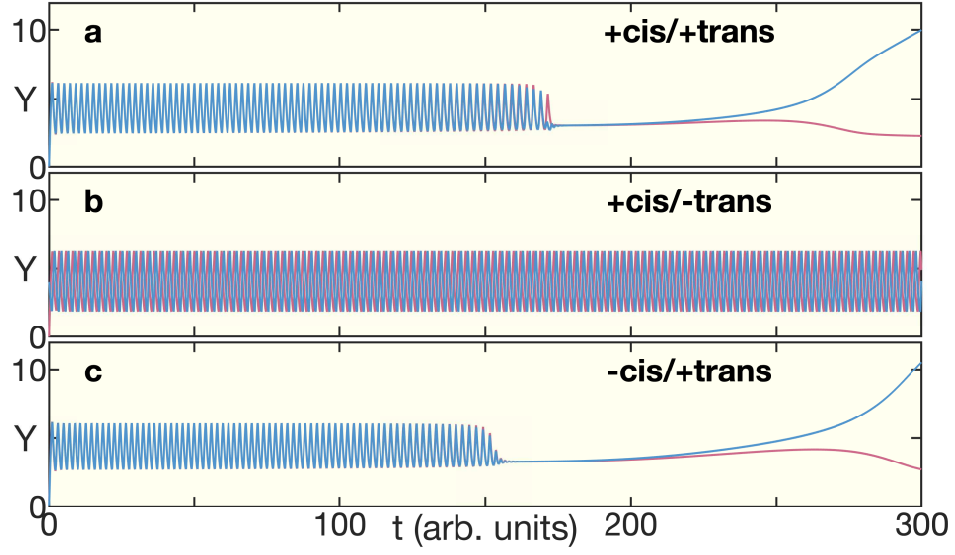


FIG. S4. **Relative importance of *trans* and *cis* forms of Notch-Delta binding for reproducing the observed sequence of transitions during somitogenesis.** The results reported in the main text assume that both forms of binding are operative with strengths $k^{\text{tr}} = k^{\text{cis}} = 1$ (a). (b) In the absence of *trans* binding (i.e., $k^{\text{tr}} = 0$), synchronized oscillations will continue indefinitely, indicating that this form of binding is crucial for the cessation of oscillations and subsequent polarization. (c) In contrast, when the *cis* form of the binding is absent (i.e., $k^{\text{cis}} = 0$), we observe no qualitative difference in the collective dynamics compared to the situation when both types of coupling are present [see (a)].

THE EFFECT OF DELAY

In order to investigate the effect of an explicit delay in the system, we incorporate a delay of duration τ_d in both (i) the regulation of X and Y by N^b and (ii) the repression of the ligand Delta by X and Y . In Fig. S5, we show the effect of increasing delay, which is expressed in terms of the relative magnitude τ_d/τ_P , where τ_P is the period of the uncoupled oscillator, on the dynamics of the system. We observe the same qualitative nature for the dynamical transitions as seen in Fig. 4 (d) of the main text, suggesting that our results are robust with respect to incorporation of signaling delays.

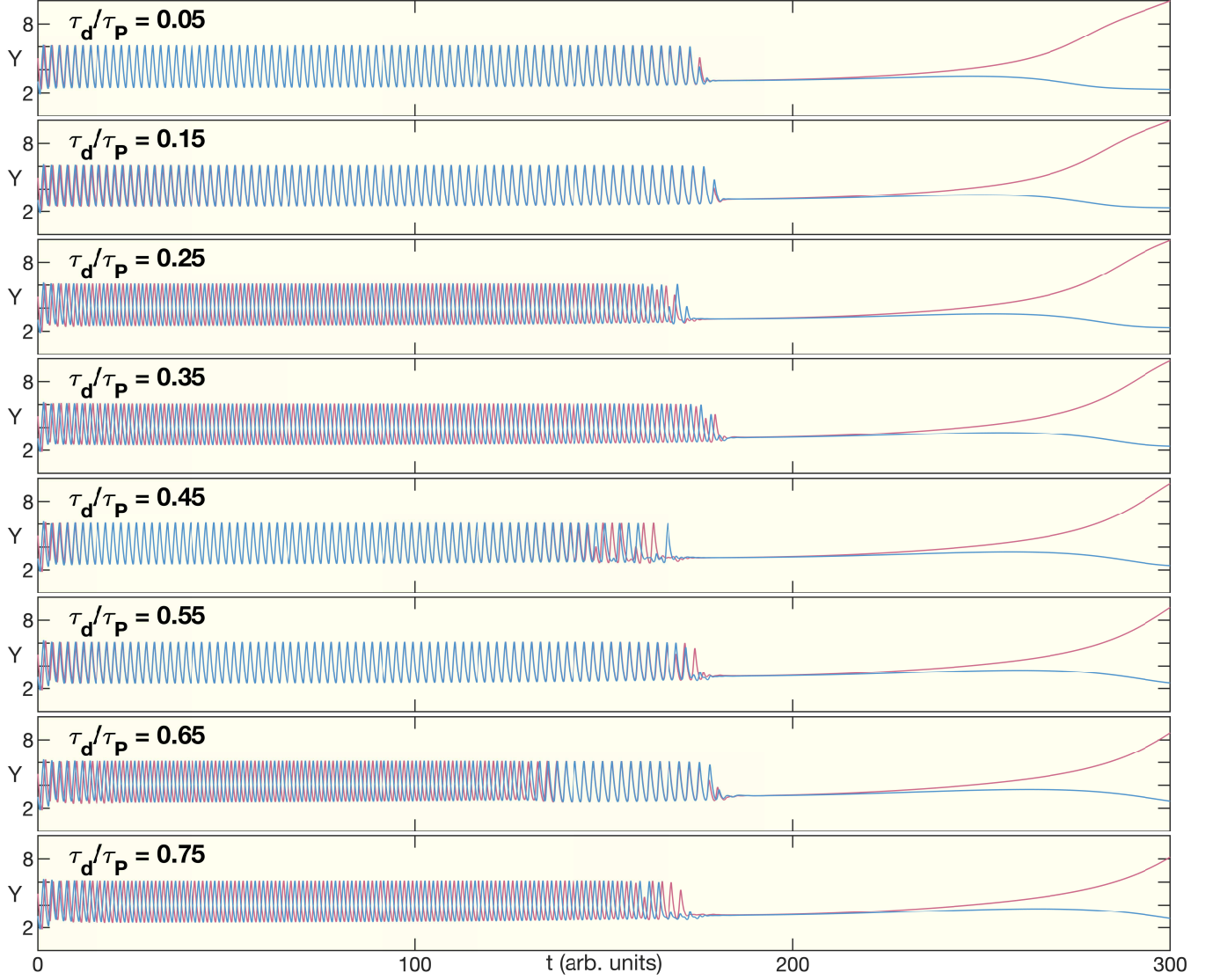


FIG. S5. Effect of delay in Notch-Delta mediated interaction on the collective dynamics of a pair of coupled oscillators responding to an exponential gradient of morphogen concentration cell signaling. The effect of the NICD (represented by the proxy variable N_b) on X and Y , as well as the effect of X and Y on the expression of the ligand Delta D , are each delayed by a period τ_d . The results shown here are obtained for a range of values of τ_d , expressed relative to τ_P , the period of an uncoupled oscillator. We observe that the transition from oscillations to an inhomogeneous steady state is unaffected by the delay.

MODELING THE MORPHOGEN GRADIENT IN A GROWING PSM

A crucial element of our model is the gradient of morphogen concentration across the presomitic mesoderm (PSM). We have explicitly considered the morphogen to be Retinoic acid (RA) whose concentration is highest at the anterior end of the PSM. Experimental evidence suggests that as the anteriorly located newly formed somites mature, each of them serve as a source of RA [3–5]. This suggests that a source, diffusion and linear degradation (SDD) model for RA will provide an appropriate description for the variation of the morphogen concentration across space and time. In particular, the source grows in strength as the number of mature somites increases over time. If one considers the PSM to be growing in discrete steps, with each new mature somite (which secretes RA at a rate ϕ) being added after a time interval τ_d , the concentration C_i of the morphogen at each putative somite in position i on the anteroposterior axis of the growing PSM can be described by the differential equation:

$$\frac{dC_i}{dt} = R(t)\delta_{i,0} + D(C_{i+1} + C_{i-1} - 2C_i) - \frac{C_i}{\tau_m},$$

where the time-varying production term $R(t)$ increases in a step-like manner by ϕ after each interval of duration τ_d , $\delta_{i,0}$ is a Kronecker delta function indicating that the source is at the anterior end of the domain (using the simplifying assumption of a point source rather than a distributed one), and D and τ_m are the effective diffusion rate and average lifetime of the RA molecules, respectively. We note that qualitatively identical results are obtained if, instead of increasing in discrete time steps, the production rate $R(t)$ changes in a continuous fashion, for example, as described by the differential equation

$$\frac{dR}{dt} = \frac{\phi}{\tau_d}.$$

Fig. S6 shows the resulting exponential profile of the morphogen concentration that will be experienced by a particular cell in the expanding PSM, which validates the use of an exponential profile for the morphogen in the main text.

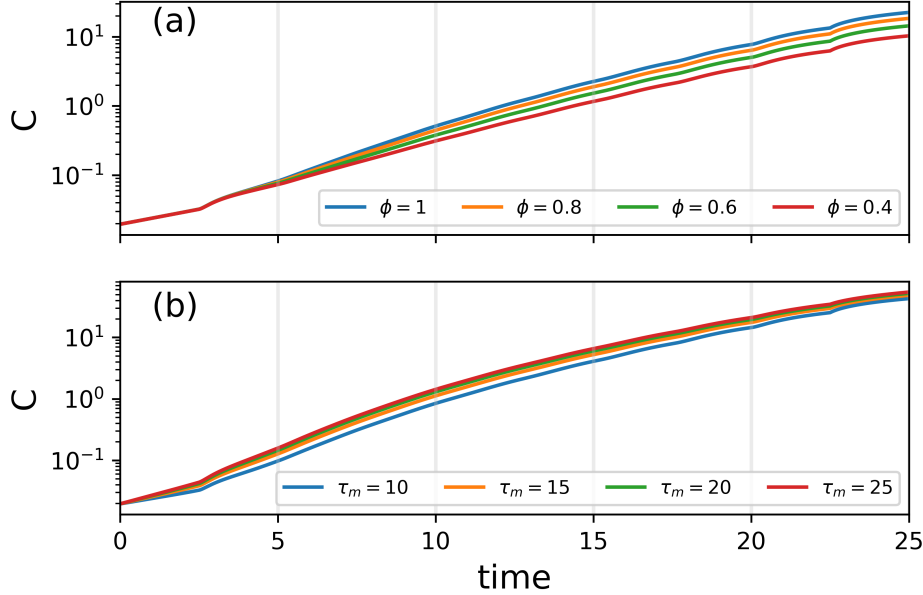


FIG. S6. **Temporal evolution of the concentration of a morphogen along the gradient as sensed by a particular cell in the growing PSM.** Concentration of the morphogen gradient as sensed by a particular cell in the growing PSM with time, shown for (a) different values of ϕ for $\tau_m = 10$, and (b) different values of τ_m for $\phi = 0.4$. The simulation domain comprises $N = 10$ putative somites at any given time, while the other parameter values are $D = 1$, $\tau_d = 5$ and $R(t = 0) = 1.0$.

TEMPORAL EVOLUTION OF ALL THE VARIABLES IN CASE OF A PAIR OF COUPLED CELLS

In the main text, the time-evolution of only one of the variables (namely, the expression of the clock gene Y) has been shown as representative of the dynamics of the system. As can be seen from Fig. S7, all the other variables also exhibit qualitatively identical behavior, with the exception of free Notch N whose production is not dependent on any of the other dynamical variables describing the state of the system.

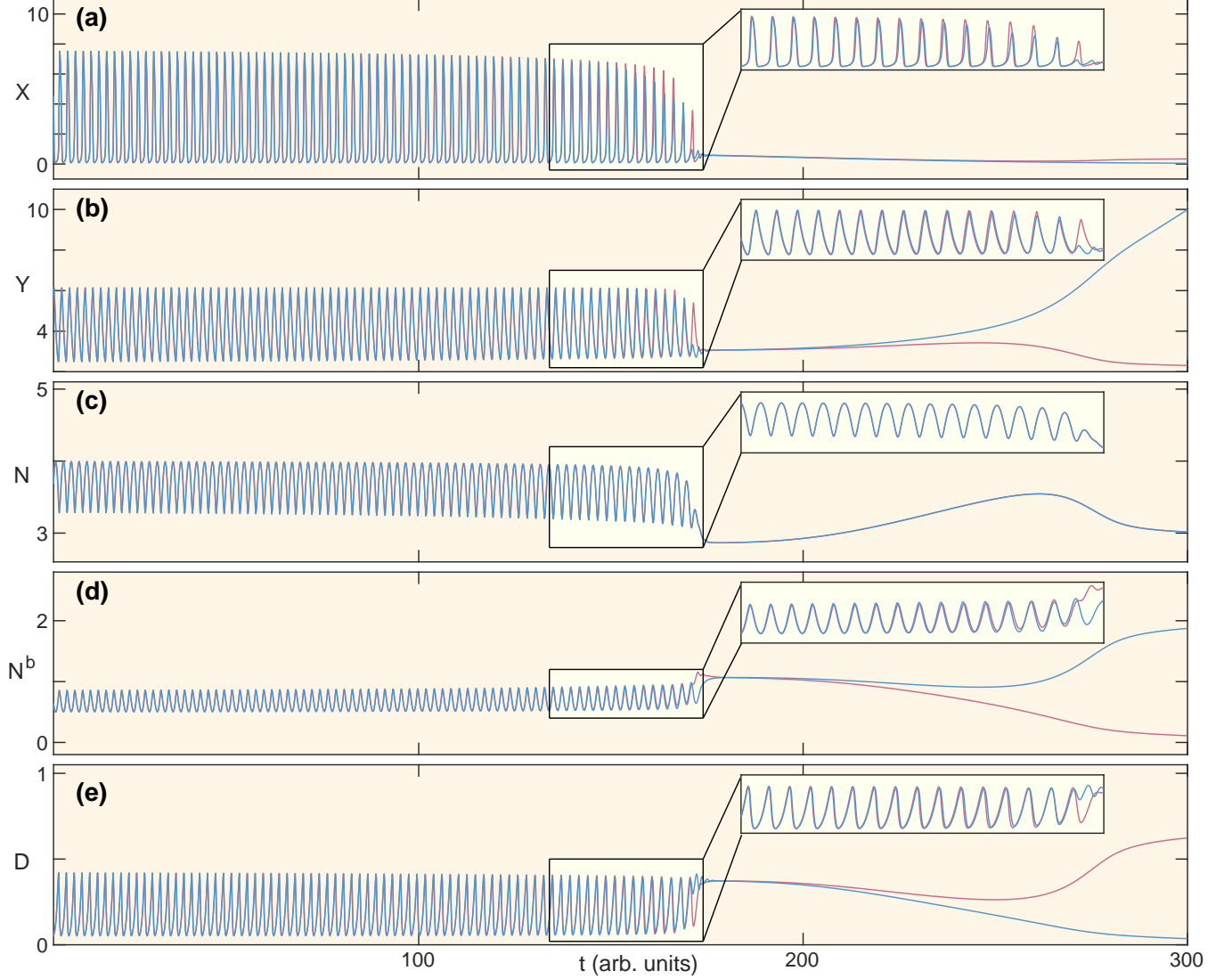


FIG. S7. **Temporal evolution of the dynamical variables in a pair of coupled oscillators responding to an exponential gradient of morphogen concentration.** Unless mentioned otherwise, the following parameter values have been used for all model simulations: $a = 16.0$, $b = 200.0$, $c = 20.0$, $e = 10.0$, $\beta^N = 5.0$, $\beta^D = 100.0$, $\gamma = 1.0$, $k^{tr} = 1.0$, $k^{cis} = 1.0$, $\mu = 1.0$, $f = 50.0$, $h = 4$, $g_{in} = 0.5$, $g_{max} = 15.0$, $dx = 3.0$ and $t_{max} = 300$.

THE EFFECT OF STEEPNESS OF THE MORPHOGEN GRADIENT

As shown in Fig. S6, the morphogen concentration increases exponentially from the posterior to the anterior along the AP axis of the PSM, such that the concentration at the position x , $g(x) \sim \exp(\lambda_g x)$. The exponent λ_g can be tuned to vary the steepness of the morphogen gradient. In Fig. S8 we consider a coupled pair of cellular oscillators separated by a distance Δx (see the schematic in Fig. 4 (a) of the main text) which are moving along the gradient. While the sequence of transitions are qualitatively identical to those shown in the main text, we observe that higher values of λ_g , which increases the slope of the gradient, results in the duration of the oscillatory regime being prolonged. More importantly, it substantially reduces the time the system spends in the transient homogeneous state prior to the ISS phase corresponding to onset of polarization. A higher value of Δx implies a larger spatial interval over which the concentration changes, which effectively alters the slope of the morphogen gradient sensed by the cells. Increasing Δx results in the ISS phase being initiated even earlier, thereby making it appear that the transition from oscillation arrest to onset of polarization is immediate.

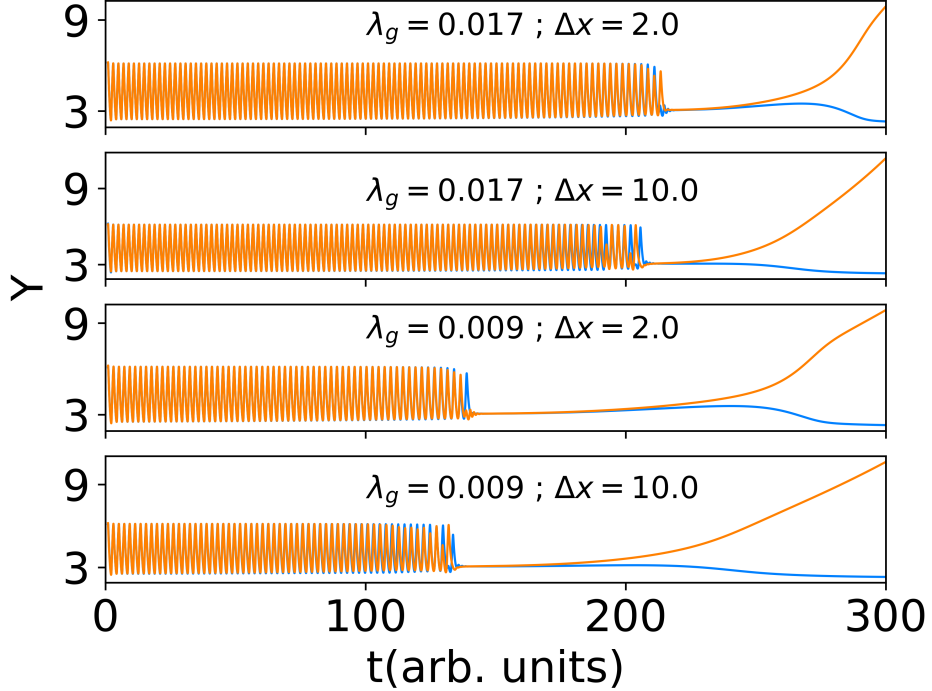


FIG. S8. **The collective dynamics of a pair of coupled oscillators separated by a distance Δx responding to an exponential gradient of morphogen concentration having steepness λ_g .** In comparison to shallower gradients (e.g., $\lambda_g = 0.009$), steeper gradients (e.g., $\lambda_g = 0.017$) prolong the oscillatory phase and correspondingly reduce the duration of HSS prior to the cells attaining different fates characterized by high and low values of protein concentration. A larger spatial separation between the centers of the two cells results in an earlier initiation of ISS, further reducing the HSS duration. Note that the qualitative features of the sequence of transitions from ES to ISS shown in Fig. 4(d) in the main text remain unchanged.

THE EFFECT OF NOISE

As gene expression is inherently noisy, it is important to verify that the sequence of transitions shown by the model introduced here are robust with respect to fluctuations in the concentrations of the relevant variables. We have, therefore, investigated the role of noise by incorporating stochasticity in the evolution equations for each of the variables X, Y, N, N^b, D . This is done by adding a term which is the product of the variable with unit Gaussian noise and a parameter θ which quantifies the strength of the noise. Fig. S9 shows that while increasing θ results in larger deviations around the mean trajectories (indicated by the thicker curves), the qualitative features of the sequence of transitions seen using the deterministic model remain invariant.

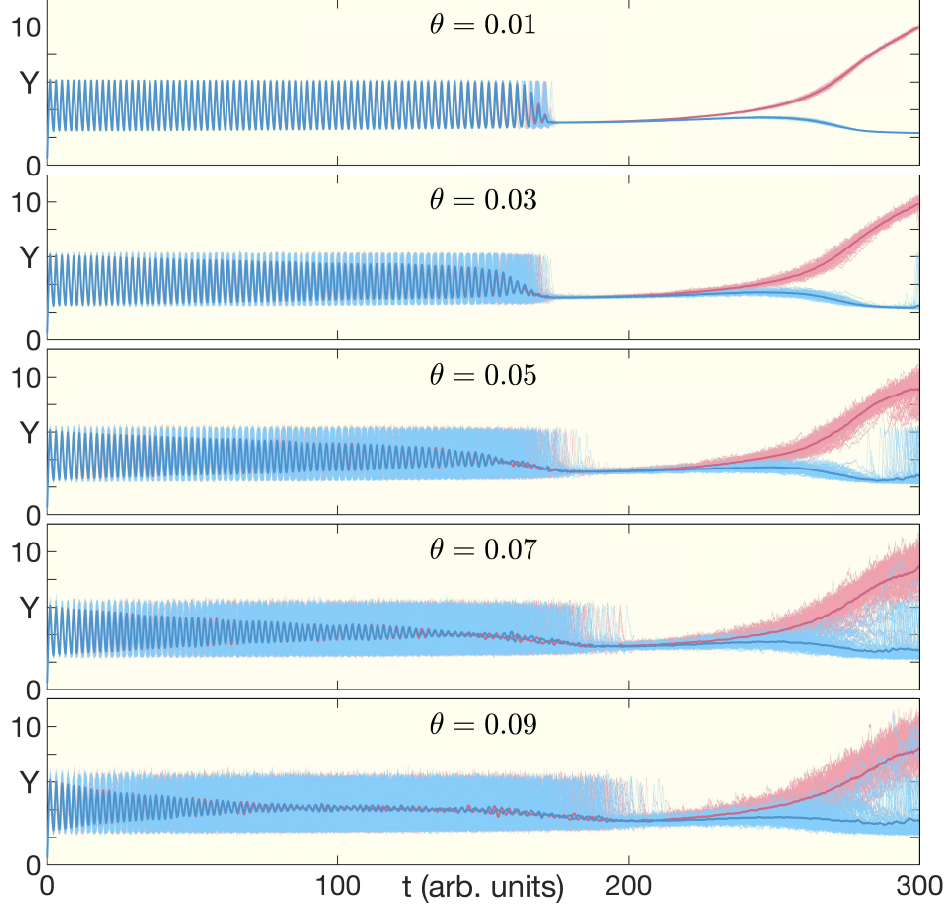


FIG. S9. **Effect of noise on the collective dynamics of a pair of oscillators interacting via Notch-Delta coupling modulated by an exponential gradient of morphogen concentration.** The evolution equation of each of the five variables $V \in \{X, Y, N, N^b, D\}$ is augmented with a noise whose variance is proportional to the instantaneous value of the corresponding variable. This is implemented by introducing an additional term which is the product of Gaussian noise $\mathcal{N}(0, 1)$ with the variable V and a parameter θ which quantifies the strength of the noise. The other parameter values used in the evolution equations are identical to that for the deterministic simulation shown in Fig. 4(d) in the main text. Each panel shows the results of 100 realizations of stochastic simulations for a given θ . The averages of these values for each cell calculated over the different realizations are the trajectories indicated using the thicker curves. We note that, although increasing noise results in higher dispersion around the mean trajectories, the qualitative features of the sequence of transitions from ES to ISS shown in Fig. 3(d) remain unchanged.

TEMPORAL EVOLUTION OF BOUND NOTCH CONCENTRATION

In the main text, the behavior of the system has been characterized by the time-evolution of expression of Y , one of the clock genes. Fig. S10 shows that a qualitatively similar picture is observed if instead one considers the time-evolution of another variable, namely, the concentration of NICD (N^b) released as a result of *trans*-activation of Notch receptors.

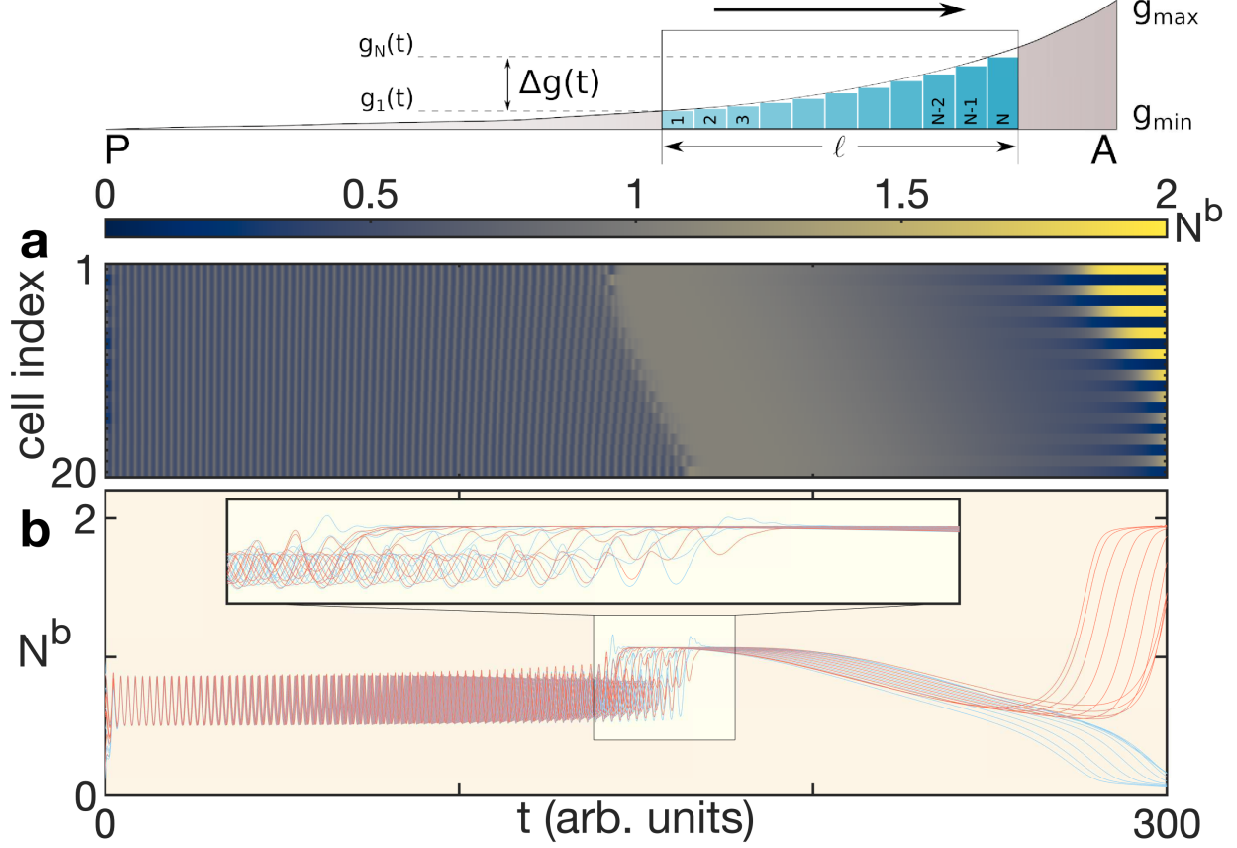


FIG. S10. **Collective dynamics of a cellular array represented in terms of the bound Notch concentration (N^b).** The collective dynamics of a cellular array comprising 20 cells responding to an exponential gradient of morphogen concentration reproduces the spatio-temporal evolution of PSM activity seen during somitogenesis, similar to Fig. 5 in the main text, but showing bound Notch (N^b) instead of the inhibitor variable Y .

THE MODEL DYNAMICS CAN GENERATE TEMPORALLY INVARIANT SPATIAL PATTERNS WITH DIFFERENT PERIODICITIES

The results reported in the main text exhibit patterns that correspond to somites, each of which comprise two cells. However, the model dynamics is capable of a richer set of possible patterns having different periodicities that can be obtained by using different values for the model parameters. This can be seen from Fig. S11 which shows a representative sample of the different types of spatio-temporal evolution leading to patterns with distinct periodicities.

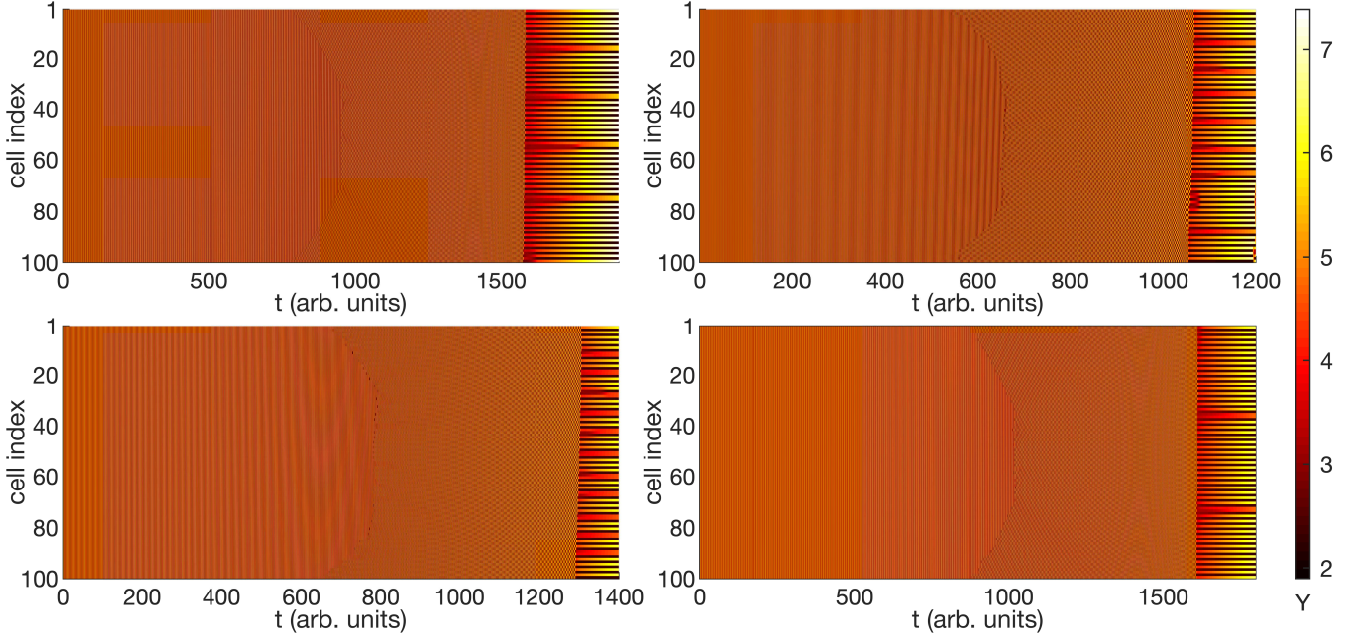


FIG. S11. The model dynamics can generate temporally invariant spatial patterns with different periodicities. ISS states that deviate from those shown in the main text are obtained by considering faster signaling dynamics, specifically, increasing the values of β^N , β^D , k^{tr} , k^{cis} , γ and μ by a factor of 10 from those used for the results reported in the main text. The different panels correspond to distinct sets of values used for the parameters f , h , g_{max} , dx and t_{max} . The patterns are shown in a 1D segment comprising $N = 100$ cells.

A TWO-DIMENSIONAL CELLULAR ARRAY CAN EXHIBIT A LINEAR SEQUENCE OF ALTERNATING PEAKS AND TROUGHS OF THE PROTEIN CONCENTRATION

In the main text we have reported only the behavior of a linear array of cells. However, we have explicitly verified that a two-dimensional array of cells which are coupled anisotropically can give rise to patterns that resemble the 1D patterns (Fig. S12). The anisotropy is a consequence of the cellular geometry, with the relatively smaller area of contact along the axis perpendicular to the AP axis resulting in a lower intensity of contact-mediated signal between cells across the transverse direction.

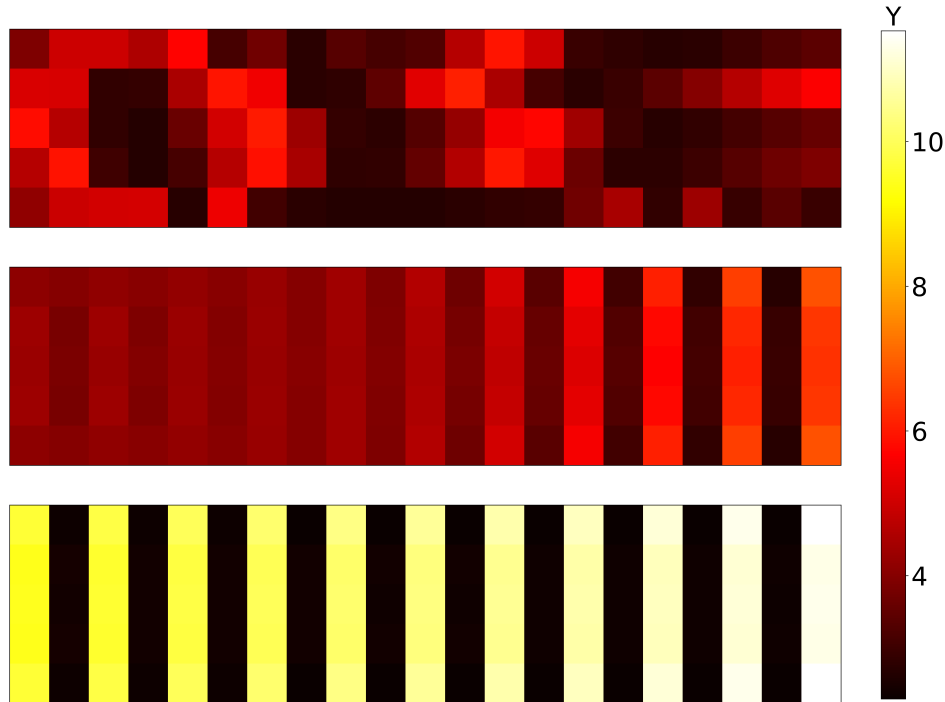


FIG. S12. **A two-dimensional cellular array can exhibit a linear sequence of alternating peaks and troughs of the protein concentration Y .** Anisotropic inter-cellular communication, which can result from the area of contact between neighboring cells being larger along the AP axis compared to that along its transverse, yields an ISS state where columns of cells aligned perpendicular to the AP axis exhibit the same concentration of Y , thereby attaining the same fate. In contrast, neighboring cells along the AP axis attain different fates characterized by high and low values of Y . The panels above show the concentration Y across the domain at different points of time, viz., (top) $t = 350$, (center) $t = 850$ and (bottom) $t = 1000$ arb. units

-
- [1] R. Guantes and J. F. Poyatos. Dynamical principles of two-component genetic oscillators. *PLoS Comput Biol*, 2:e30, 2006.
 - [2] D. Sprinzak, A. Lakhanpal, L. LeBon, L. A. Santat, M. E. Fontes, G. A. Anderson, J. Garcia-Ojalvo, and M. B. Elowitz. Cis-interactions between notch and delta generate mutually exclusive signalling states. *Nature*, 465(7294):86, 2010.
 - [3] R. D. del Corral, I. Olivera-Martinez, A. Goriely, E. Gale, M. Maden, and K. Storey. Opposing fgf and retinoid pathways control ventral neural pattern, neuronal differentiation, and segmentation during body axis extension. *Neuron*, 40(1):65–79, 2003.
 - [4] R. D. del Corral and K. G. Storey. Opposing fgf and retinoid pathways: a signalling switch that controls differentiation and patterning onset in the extending vertebrate body axis. *Bioessays*, 26(8):857–869, 2004.
 - [5] M. Rhinn and P. Dollé. Retinoic acid signalling during development. *Development*, 139(5):843–858, 2012.